Dental Materials 40 (2024) 1937–1953

Contents lists available at ScienceDirect

Dental Materials

journal homepage: www.elsevier.com/locate/dental

Polymer vesicles for the delivery of inhibitors of cariogenic biofilm

Parmanand Ahirwar [a,1,2], Veronika Kozlovskaya [a,1,3], Piyasuda Pukkanasut [a], Pavel Nikishau [a,4], Sarah Nealy [a], Gregory Harber [b], Suzanne M. Michalek [b], Linto Antony [c], Hui Wu [g,5], Eugenia Kharlampieva [a,d,*,6], Sadanandan E. Velu [a,e,f,*,7]

[a] Department of Chemistry, University of Alabama at Birmingham, Birmingham, AL 35294, USA
[b] Department of Microbiology, University of Alabama at Birmingham, Birmingham, AL 35294, USA
[c] Department of Medicine, University of Alabama at Birmingham, Birmingham, AL 35294, USA
[d] Center of Nanoscale Materials and Biointegration, University of Alabama at Birmingham, Birmingham, AL 35294, USA
[e] Microbiome Center, Center, University of Alabama at Birmingham, Birmingham, AL 35294, USA
[f] Global Center for Craniofacial Oral and Dental Disorders, University of Alabama at Birmingham, Birmingham, AL 35294, USA
[g] Department of Integrative Biomedical and Diagnostic Sciences, Oregon Health and Science University, Portland, OR 97239, USA

ARTICLE INFO

Keywords:
Dental caries
Streptococcus mutans
Biofilm
Glucosyl transferase
PH-responsive
Polymersome

ABSTRACT

Objectives: The goal of this study is to develop a novel drug delivery platform for the pH-responsive delivery of biofilm inhibitors as a potential avenue to prevent and treat dental caries.
Methods: Biofilm and growth inhibition assays were performed in polystyrene microtiter 96-well plates. Docking analysis was performed using the reported GtfB + HA5 co-crystal structure (PDB code: 8fg8) in SeeSAR 13.0.1 software. Polymersome vesicles were assembled from poly(N-vinylpyrrolidone)$_8$-*block*-poly(dimethylsiloxane)$_{64}$-*block*-poly(N-vinylpyrrolidone)$_8$ (PVPON$_8$-PDMS$_{64}$-PVPON$_8$) triblock copolymer using a nanoprecipitation method. Microbiome analysis of biofilm inhibitors and the *in vivo* drug release and antivirulence activities of polymersome encapsulated inhibitors have been carried out in a *S. mutans* induced rat caries model.
Results: Biofilm inhibitors for HA5 and HA6 have shown species-specific selectivity towards *S. mutans* and the ability to preserve the oral microbiome in a *S. mutans* induced dental caries model. The inhibitors were encapsulated into pH-responsive block copolymer vesicles to generate polymersome-encapsulated biofilm inhibitors, and their biofilm and growth inhibitory activities against *S. mutans* and representative strains of oral commensal streptococci have been assessed. A 4-week treatment of *S. mutans* UA159 infected gnotobiotic rats with 100 μM of polymersome-encapsulated biofilm inhibitor, PEHA5 showed significant reductions in buccal, sulcal, and proximal caries scores compared to an untreated control group.
Significance: Taken together, our data suggests that the biofilm-selective therapy using the polymersome-encapsulated biofilm inhibitors is a viable approach for the prevention and treatment of dental caries while preserving the oral microbiome.

Abbreviations: ANOVA, Analysis of variance; BTB, Bis-Tris; BAP, Blood agar plate; CDM, Chemically defined medium; CFU, Colony forming unit; DNA, Deoxyribonucleic acid; DMSO, Dimethyl sulfoxide; EPS, Extracellular polysaccharide; Gtf, Glucosyltransferases; HPLC, High performance liquid chromatography; IC50, Half maximal inhibitory concentration; KD, Dissociation constant; MS, Mitis-Salivarius agar; OTU, Operational taxonomic unit; PCR, Polymerase chain reaction; ppm, Parts per million; qPCR, Quantitative polymerase chain reaction; RNA, Ribonucleic acid; SEM, Standard error of the mean; SDS-PAGE, Sodium dodecyl sulfate-polyacrylamide gel electrophoresis; *S. gordonii*, *Streptococcus gordonii*; *S. mutans*, *Streptococcus mutans*; *S. sanguinis*, *Streptococcus sanguinis*; THB, Todd Hewitt Broth.

* Corresponding authors at: Department of Chemistry, University of Alabama at Birmingham, Birmingham, AL 35294, USA.
E-mail addresses: ekharlam@uab.edu (E. Kharlampieva), svelu@uab.edu (S.E. Velu).
[1] Contributed equally to this manuscript.
[2] orcid.org/0000-0003-1910-5016
[3] orcid.org/0000-0001-9089-4842
[4] orcid.org/0000–0002-2473-4821
[5] orcid.org/0000-0003-1694-3954
[6] Orcid.org/0000-0003-0227-0920
[7] Orcid.org/0000-0002-0342-2378

https://doi.org/10.1016/j.dental.2024.09.006
Received 14 June 2024; Received in revised form 6 September 2024; Accepted 10 September 2024
Available online 23 September 2024

1. Introduction

Dental caries, commonly known as tooth decay, is a ubiquitous bacterial infectious disease that causes demineralization of enamel and dentin [1]. A recent Lancet study of global burden of 328 major diseases recognizes dental caries as the most prevalent disease worldwide [2]. Although dental plaque contains more than 700 bacterial species living in complex bacterial communities called biofilms, the gram-positive bacterium *Streptococcus mutans,* characterized by its ability to form tenacious biofilms is considered to be the primary etiological agent for this disease [3,4]. Biofilm formation is initiated by the attachment of commensal *streptococci* such as *Streptococcus sanguinis* and *Streptococcus gordonii* to the tooth surface and the subsequent intra- and inter-species microbial interactions [5–7]. Low numbers of cariogenic bacteria often live together with their benign commensal counterparts in the oral cavity as multispecies biofilm communities [8–10]. Under the disease conditions, pathogenic bacteria overgrow the commensals disturbing the delicate balance between them [11,12]. Current antimicrobial treatments for dental caries such as oral rinses affect both pathogenic and commensal bacteria alike. Therefore, it would be beneficial if the studies aimed at developing new caries treatments focus on identifying antibiofilm agents that have no adverse impact on the growth of oral commensal species. One of the strategies to accomplish this goal is by developing inhibitors of *S. mutans* virulence factors such as extracellular glucosyl transferases (Gtfs) [13]. *S. mutans'* secreted enzymes GtfB and GtfC are primarily responsible for the synthesis of water-insoluble glucans [14,15] and GtfD is responsible for the synthesis of water-soluble glucans [16,17]. Functions of *S. mutans* Gtfs are essential for glucan synthesis, biofilm formation and the resulting cariogenesis [13]. Therefore, inhibiting *S. mutans* Gtfs is an excellent strategy to specifically inhibit its biofilm without affecting its viability and the viability of oral commensal bacterial species. Two such Gtf inhibitors reported from our lab are compounds HA5 and HA6 [18].

The goal of the present study is to encapsulate HA5 or HA6 in pH-responsive polymer nanoplatforms and explore their on-demand pH-responsive delivery in the oral cavity to prevent or treat dental caries. The pH-responsive delivery of antibacterial agents is a desirable approach to treat dental caries as the pH level in oral cavity is one of the critical factors contributing to the demineralization process of tooth enamel. The human salivary system maintains a healthy non-harmful pH of 6.0 – 7.5 in the oral cavity [19,20] under physiological conditions controlled by three buffer systems: 1) bicarbonate, 2) phosphate and 3) salivary proteins [21,22]. Under pathogenic oral conditions, biofilm ferments the dietary carbohydrates to produce acidic byproducts such as lactic acid leading to a drop in salivary pH to < 5.5, which is harmful to the tooth enamel and dentin [21–24]. Therefore, dental caries treatment would tremendously benefit from an antibiofilm agent that is delivered on the tooth surface as the pH drops below 5.5.

Given the challenges of poor solubility of small molecule antibacterial agents, difficulty of penetration into biofilms, and lack of retention of the drugs within biofilm, the use of nanomaterials for the localized delivery of antibacterial agents is a prudent approach to treat dental caries [25–29]. Examples of such studies are the delivery of farnesol and myricetin using nanoparticle carriers to inhibit biofilm [30], delivery of farnesol using pH-responsive micelles (PPi-Far-PM) [31] and the use of nano systems such as mesoporous silica nanoparticle (MSN) [32,33], liposome [34], halloysite nanotube (HNT) [35], and polyamidoamine (PAMAM) [36] for controlled release of anticaries drugs. However, none of these approaches have been translated to clinical use so far as their *in vivo* efficacies are either modest or unproven.

Our interest is focused on developing a novel polymersome drug delivery system with built-in pH-sensitivity for the delivery of biofilm inhibitors. Polymersomes are hollow polymeric spheres with an aqueous core and a polymer membrane that has close similarity to the membrane of liposomes [37,38]. Polymersomes are ideal delivery platforms for small-molecule biofilm inhibitors as their amphiphilicity makes them capable of encapsulating both hydrophilic and hydrophobic molecules in their core and polymer shell, respectively [39]. Polymersomes are mechanically robust with efficient drug loading capacity and ability to respond to environmental stimuli such as pH or temperature [40–42]. Such polymer vesicles made from block copolymers of polybutadiene-b-poly(L-glutamic acid) and polyethyloxide-β-polycaprolactam have been shown to release their cargo through the vesicle disassembly due to the presence of the degradable bonds within their structure [42]. We specifically designed spherical block copolymer vesicles to encapsulate our biofilm inhibitors. These hollow vesicles were self-assembled from poly(N-vinylpyrrolidone)$_8$-*block*-poly(dimethylsiloxane)$_{64}$-*block*-poly(N-vinyl-pyrrolidone)$_8$ (PVPON$_8$-PDMS$_{64}$-PVPON$_8$) block copolymer into ~30-nm spherical hollow nanovesicles *via* a nanoprecipitation method. The synthesis of these nanovesicles was carried out by the reversible addition-fragmentation chain transfer (RAFT) polymerization we have reported previously [43]. Due to the presence of acid-labile ester (–COO–) linkages between PDMS and PVPON blocks, the assembled polymersome vesicles are degraded at pH < 4 and release the cargo [43].

2. Materials and methods

2.1. General considerations

All bacterial strains (*S. mutans* UA159, *S. gordonii* DL1, and *S. sanguinis* SK36) were inoculated statically at 37 °C under 5 % CO_2 environment in Todd Hewitt Broth (THB) for 24 h [44]. The cultures were then diluted with fresh THB (1:5) and reinoculated until the optical density at 470 nm reaches 1. The optical density was read using BioTek 800 TS absorbance reader at 470 nm for bacterial growth and 562 nm for biofilm stained with crystal violet. Data was plotted in Prism 10.0.2. TEM images of polymersome vesicles assembled from PVPON$_8$-PDMS$_{64}$-PVPON$_8$ were obtained using a FEI Tecnai T12 Spirit TWIN TEM microscope operating at 80 kV. For imaging, 7 μL of the vesicle solution was deposited onto an argon plasma-treated Formvar/carbon-coated copper grid (400 mesh, Electron Microscopy Sciences). After 30 s the excess vesicle solution was blotted, and the adsorbed vesicles were then stained with 1 wt% uranyl acetate. The excess staining solution was immediately blotted prior to imaging.

2.2. Biofilm inhibition assays

Biofilm inhibition assays were performed in polystyrene microtiter 96-well plates. Stock solutions were prepared in chemically defined medium (CDM) with 1 % sucrose, 1 % bacteria cultures and various concentrations of the small molecule inhibitors to examine their activity against biofilm formation as described [45,46]. These stocks were assayed in 96 well plates in triplicate and incubated at 37 °C and 5 % CO_2 for 16 h. After reading optical density for bacterial growth, the plate was washed, dried, and stained with 0.1 % crystal violet which was again rinsed well with deionized water leaving the stained biofilm at the bottoms of the wells. This biofilm was dissolved in 200 μL of 30 % acetic acid and absorbance at 562 nm was read to determine amount of biofilm formation. Each assay was carried out at least in triplicate. Biofilm inhibitor concentration (IC_{50}) of the compounds was determined by serial dilutions from 0 μM – 50 μM (1 % DMSO).

2.3. S. mutans, S. gordonii, and S. sanguinis growth assays

Effects of PEHA5, PEHA6, HA5 and HA6 on *S. mutans* and commensal bacterial growth were evaluated using the growth assay as described [45]. *S. mutans* UA159, *S. gordonii* DL1, *S. sanguinis* SK36, cultures were grown for 24 h under 5 % CO_2 at 37 °C. These cultures were then reinoculated with fresh THB (1:5) until $OD_{470} = 1$ when the bacteria were ready to be used. Different concentrations of the PEHA5, PEHA6, HA5 and HA6 were assayed in CDM with 1 % of the bacteria, 1 % sucrose

and 1 % DMSO in 96 well plates. The 96 well plates were incubated under 5 % CO_2 at 37 °C for 16 h. Growth of the bacteria was read after 16 h at OD_{470}. Each assay was carried out at least in triplicate.

2.4. Gtf inhibition is determined by glucan quantification assays

Gtf inhibition assays were performed to assess the ability of HA6 to inhibit the Gtfs and glucan production using a reported procedure and IC_{50} value was calculated [47,48]. Overnight cultures of *S. mutans* UA159 were centrifuged (6500 rpm, 4 °C, 10 min) to remove the cells. Supernatant was mixed with ethanol (1:1) and incubated at −80°C for 1 h. The precipitated Gtfs were palleted using centrifugation and resuspended in CDM (1 mL). 10 μL of Gtfs suspension in CDM was assayed on Ibidi slides with varying concentrations of HA6, 1 % sucrose, 1 % DMSO and 1 μM Cascade blue dextran conjugated dye in CDM. The slides were then incubated at 37 °C with 5 % CO_2 for 16 h after which, the wells of Ibidi slides were gently rinsed with 1x PBS and imaged using fluorescence microscopy. The images obtained were processed in ImageJ to quantify glucans and graphed in GraphPad Prism 10.0.2.

2.5. Docking analysis

The reported GtfB + HA5 co-crystal structure (PDB code: 8fg8) was downloaded from protein databank [18]. Chain B of the protein was selected for the docking, water molecules and sulfate ions were removed using PyMol [49]. Bis-Tris (BTB) molecule and calcium ions that are close to the binding site and contribute significantly to the free energy of binding (ΔG_{HYDE}) of the inhibitor HA5 toward GtfB were kept. The protein was loaded into SeeSAR 13.0.1 [50] and all residues within a 6.5 Å radius around the ligand, HA5 were automatically selected to use as a binding site for the docking study. The ligand HA5 was exported to SeeSAR docking mode and the compound HA6 in sdf format was uploaded to SeeSAR using a templated docking mode. The docking was carried out using FlexX 6.0.0 integrated in SeeSAR 13.0.1[51,52]. The estimated affinities, torsions, and clashes were calculated for all poses in SeeSAR analyzer mode. The pose of HA6 which has the least torsion, no intra and inter molecular clashes was selected as the primary docking mode of the molecule within the GtfB active stie.

2.6. Encapsulation of HA5 into polymer vesicles

HA5 loaded polymersomes were prepared using a nanoprecipitation method. For that, 1.0 mL of the $PVPON_8$-$PDMS_{64}$-$PVPON_8$ triblock-copolymer solution in ethanol (5.0 mg/mL) was added dropwise to 4.0 mL of the 2.5 mg HA5 (or HA6) solution in DI water at room temperature and left under stirring for 2 h. Then, the obtained solution was dialysed in DI water for 48 h using a Float-a-Lyzer (MWCO 1000 Da, Fisher Scientific) to remove ethanol, followed by dialysis in DI water for 72 h using a Float-a-Lyzer (MWCO 100 kDa, Fisher Scientific) to remove an excess of the drug. The hydrodynamic size of empty and encapsulated polymersomes was measured using a Nano-ZS Zetasizer (Malvern Panalytical) equipped with a He–Ne laser (663 nm) at 25 °C. Drug concentration was calculated using a NanoDrop One Microvolume UV-Vis spectrophotometer (Thermo Fisher).

2.7. Impact of HA5 and HA6 on the rat oral microbiome

We used Fischer 344 rats that were bred and maintained in trexler isolators for this experiment. Male and female rat pups were removed from isolators at 20 days of age and randomly assigned into treatment groups of 5 rats / group in cages with filter tops. Rats were then infected with *S. mutans* UA159 strain by oral swabbing daily for four consecutive days with a fresh overnight culture of *S. mutans* UA159. Rats were provided with caries promoting Teklad Diet 305 containing 5 % sucrose (Harlan Laboratories, Inc., Indianapolis, IN) and sterile drinking water *ad libitum*. Oral swabs were taken 5 days post-infection and plated on Todd Hewitt (TH) agar plates and incubated at 37 °C in an environment of 5 % CO_2 in the air to confirm colonization. Rats were weighed at weaning and then weekly throughout the experiment. One-week post-infection, the molars of the rats were brushed twice daily for 4 weeks with the test compounds using camel-hair brushes. Four treatment groups used in this study were: 1) HA5 (100 μM); 2) HA6 (100 μM); 3) NaF (250 ppm); and 4) infected untreated rats. Drinking water was withheld for 60 min following each treatment with the compound. Animals were weighed at weaning and at the termination of the experiment. On day 60, the rats were sacrificed using CO_2 followed by cervical dislocation or bilateral thoracotomy. The mandibles were surgically removed and cleaned of excess tissue to assess the level of bacteria present and the extent of caries formation. The right mandible from each rat was placed in a tube containing phosphate buffer (3 mL), placed on ice and sonicated (10 s) to release bacteria from the molars. Each sample was serially diluted, plated on blood (BAP) and mitis-salivarius (MS) agar plates and incubated in an environment of 5 % CO_2 in air at 37 °C to quantify the level of total bacteria and *S. mutans* present in the plaque. The right and left mandibles from each rat were then placed in 95 % ethanol for 24 h. The mandibles were cleaned and stained overnight with murexide solution. After drying, the mandibles were sectioned and scored for caries activity using the Keyes method [53]. Caries scores were recorded for the buccal, sulcal and proximal molar surfaces individually so that differences among the surfaces can be distinguished. Statistical significance in the mean caries scores, colony-forming units (CFU)/mandible and body weights between groups of rats were determined by one-way analysis of variance (ANOVA) with the Tukey-Kramer multiple comparison test using the InStat program (GraphPad Prism 10.0.2.). When determining the statistical significance between the two groups, an unpaired t-test was applied. Differences between groups were considered significant at a P-value < 0.05.

In addition to recording buccal, sulcal and proximal molar surface caries scores and colony-forming units (CFU)/mandible and body weights between groups of rats as described above, plaque samples from rats treated or untreated were collected and DNA was extracted from each sample and used for PCR amplification of ~430 bp amplicons of 16S ribosomal DNA hypervariable regions V3 and V4, Illumina adaptors, and molecular barcodes as described [54]. Barcoded PCR samples were sequenced at UAB Microbiome Research Core. The Ribosomal Database Project classifier was used to assign a taxonomic classification to each read in the representative set and a phylogenetic tree will be constructed from the representative sequences. The relative abundance of each OTU was examined at phylum, class, order, family, genus, and species levels. Alpha and beta diversity analysis of the oral microbial community was performed using MicrobiomeAnalyst 2.0 [55]. The ASV table containing the raw counts was filtered to remove low abundance features that were less than 10 % prevalence in samples, and data scaling was performed using Total sum scaling (TSS) prior to the diversity analysis. Alpha diversity indices generated were used in GraphPad Prism 10.0.2 to generate the bar plots. All experimental protocols were approved by the University of Alabama at Birmingham Institutional Animal Care and Use Committee. The methods were carried out in accordance with the relevant guidelines and regulations.

3. Results

3.1. Biofilm inhibitors HA5 and HA6

Biofilm inhibitors HA5 and HA6 (Fig. 1) are excellent candidates for polymersome encapsulation as they inhibited *S. mutans* biofilm with IC_{50} values of 6.42 μM and 18.92 μM, respectively without affecting the growth of commensal species *S. gordonii* and *S. sanguinis* at their biofilm inhibiting doses. They were also found to have solubilities of 120.09 μg / mL and 90.77 μg / mL, suitable for encapsulation into polymersome vesicles. Both inhibitors HA5 and HA6 were synthesized in large scale using the synthetic protocols reported from our lab recently [18].

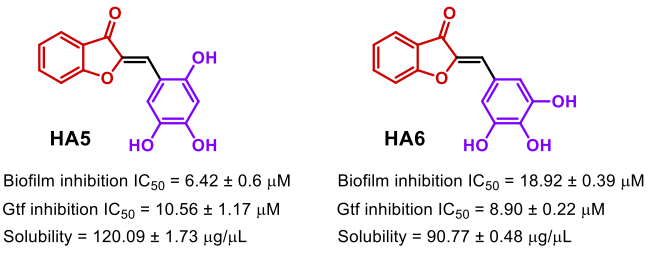

Fig. 1. Inhibitors of *S. mutans* glucosyl transferases and biofilm.

Detailed evaluation of Gtf inhibition, biofilm inhibition and growth inhibition activities of compound HA5 has already been reported in our prior publication [18]. Additional *in vitro* and *in vivo* evaluations were conducted for compound HA6 to ensure its suitability for encapsulation as described in the following sections.

3.2. Biofilm and growth inhibition by HA6

Compound HA6 inhibited *S. mutans* biofilm in a dose dependent manner with an IC_{50} value of 18.92 ± 0.39 μM (Fig. 2A). Staining of bacterial cells within biofilms with Syto-9 showed significant reduction in biofilms at 15 μM and a complete inhibition at 30 μM of HA6 (Fig. 2E-I). The presence of glucans, which were stained with Cascade Blue-dextran conjugated dye, was significantly reduced at 15 μM and no glucan formation was evident at 30 μM of HA6 (Fig. 2E-II). In addition, propidium iodide was used to determine the presence of extracellular DNA (eDNA) in *S. mutans* biofilms. Again, there was a noticeable reduction of eDNA at 15 μM and almost complete absence of eDNA at 30 μM of HA6 (Fig. 2E-III). These findings reaffirm that compound HA6 inhibited *S. mutans* biofilms by preventing the synthesis of glucans and minimizing the presence of eDNA, two integral biofilm matrix elements crucial for *S. mutans* biofilm formation.

To determine if HA6 only selectively inhibits *S. mutans* biofilms without affecting the planktonic growth of *S. mutans* and oral commensal species, the effects of HA6 on the viability of two representative oral commensal streptococci, *S. gordonii* and *S. sanguinis*, along with *S. mutans* at 25 μM and 50 μM doses were evaluated. As shown in Fig. 2B, compound HA6 did not inhibit the growth of *S. sanguinis*, while it showed about 10 % inhibition of the growth of *S. gordonii* compared to the control groups at these doses that are much higher than its biofilm IC_{50} value of 18.92 μM. Similarly, the compound HA6 did not inhibit *S. mutans* viability at these doses (Fig. 2B). In addition, we have demonstrated that HA6 did not significantly reduce the biofilms of the commensal species *S. gordonii* and *S. Sanguinis* at 25 μM (Fig. 2C-D).

3.3. Gtf binding and inhibition by HA6

Gtf inhibition assays were performed to assess the ability of HA6 to inhibit the Gtfs and glucan production using a reported procedure [47, 48] and the IC_{50} value was determined to be 8.90 ± 0.22 μM (Fig. 3A). In order to predict the interactions of HA6 within GtfB active site and further support its mechanism of action, we performed a docking analysis of HA6 using our recently published X-ray crystal structure of the catalytic domain of GtfB co-crystallized with HA5 (PDB: 8fg8) [18]. The

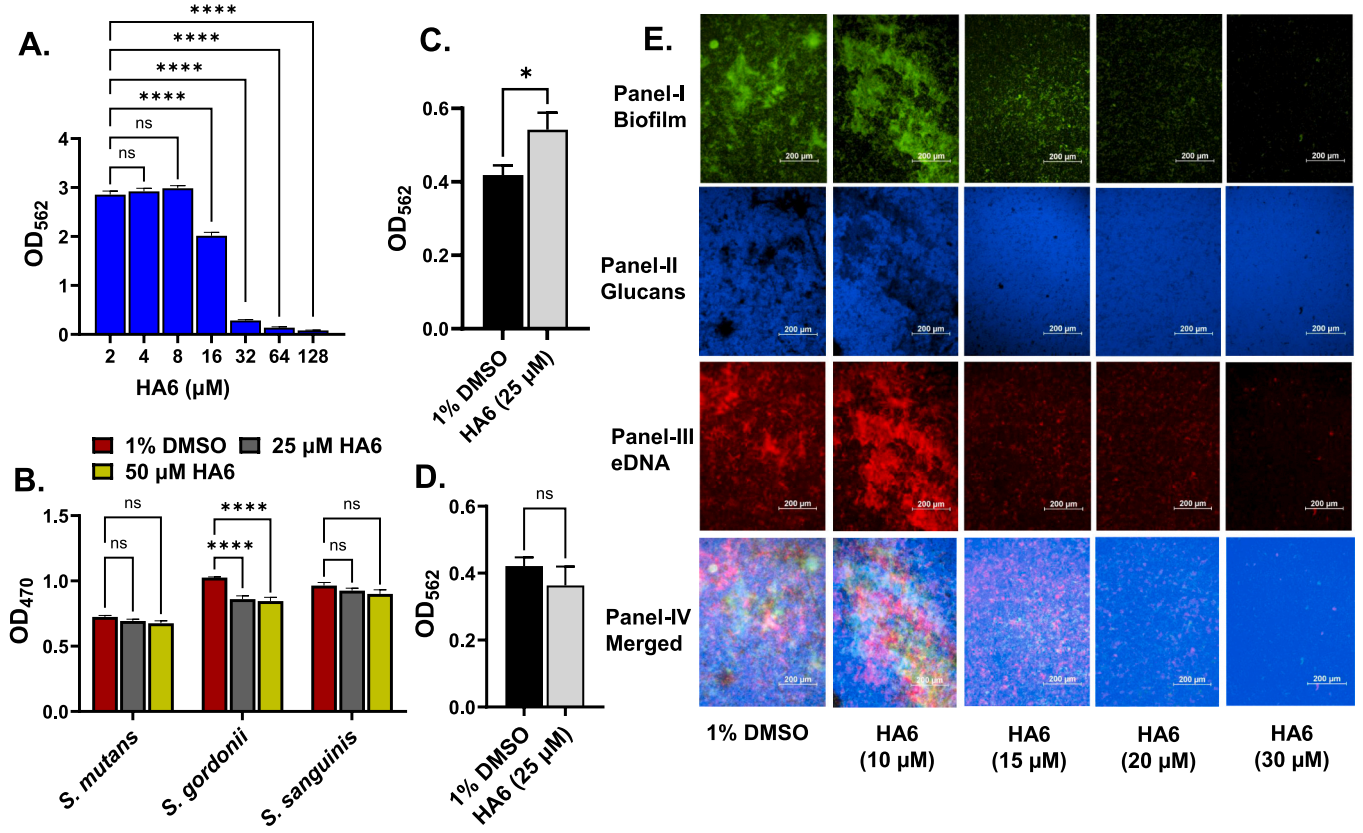

Fig. 2. Biofilm and growth inhibitory activities of the compound HA6. A) *S. mutans* UA159 were co-incubated with HA6 at various concentrations and biofilm formation was measured at OD_{562} using the crystal violet protocol and IC_{50} value was determined. B) *S. mutans* UA159, *S. gordonii* DL1 and *S. sanguinis* SK36 were co-incubated with HA6 at 25 μM and 50 μM and their planktonic growth were measured at OD_{470}. C) *S. gordonii* DL1 were co-incubated with HA6 at 25 μM and biofilm formation was measured at OD_{562} using the crystal violet protocol. D) *S. sanguinis* SK36 were co-incubated with HA6 at 25 μM and biofilm formation was measured at OD_{562} using the crystal violet protocol. E) Representative fluorescence microscopy images of UA159 biofilms after 16 h of treatment with various concentrations of HA6. Bacterial cells were stained with Syto-9 (green, panel-I); glucans were stained with Cascade Blue dextran conjugated dye (blue, panel-II); eDNA was stained with propidium iodide (red, panel-III), and a merged image of all three staining images (panel-IV).

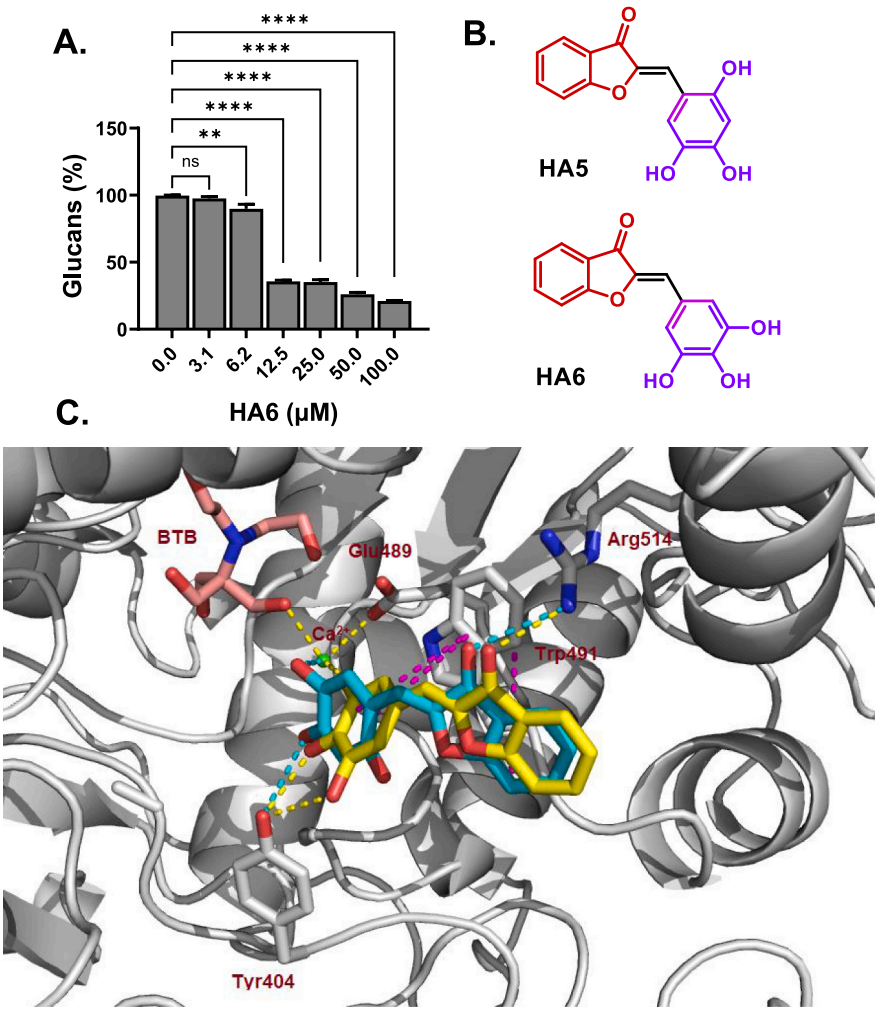

Fig. 3. Gtf inhibitory activities of the compound HA6. A) Gtfs precipitated from *S. mutans* UA159 culture were co-incubated with HA6 at various concentrations and the glucan production was quantified using Cascade Blue dextran conjugated dye staining and subsequent image processing with ImageJ. B) Chemical structures of HA5 and HA6. C) Interactions of HA6 (yellow sticks) within GtfB active site predicted by docking carried out using FlexX6.0 suite with SeeSAR 13.0.1 software compared with the HA5 (cyan sticks, PDB: 8fg8).

docking analysis was carried out using FlexX6.0 suite with SeeSAR 13.0.1 software [50–52].

The GtfB binding of HA6 is expected to be similar to HA5 as their chemical structures are very similar with only a difference in the position of one OH group on the trihydroxyphenyl ring. The compound HA5 contained a 2,4,5-trihydroxyphenyl ring, while HA6 contained a 3,4,5-trihydroxyphenyl ring. An overlay of HA6 docking model with the crystal structure of HA5 and their key active site interactions are presented in Fig. 3C. There are two H-bonding interactions noticed for HA6 within GtfB active site, one through 3,4-OH groups of the 3,4,5-trihydroxyphenyl moiety with Tyr404. The second H-bonding interaction of HA6 was with the carbonyl O atom present in the 5-membered ring with the guanidine side chain of Arg514. Similar H-bonding interactions were also observed in the crystal structure of HA5 at the 4-OH position from the 2,4,5-trihydroxyphenyl moiety and with the O atom of the carbonyl group of the 5-membered ring. The 3-OH group of both HA6 and HA5 displayed indirect interactions with the amino acid residue Glu489 through a conserved Ca^{2+} ion, which also interacted with BTB, a component of buffer used in crystallization studies [56]. Like the crystal structure of HA5, the docking model of HA6 also had electrostatic and π–π stacking interactions with Trp491 in the GtfB active site. Overall, our docking analysis and the Gtf inhibition data suggest that the inhibitor HA6 can effectively inhibit the Gtf activity like HA5.

3.4. Effect of HA5 and HA6 on rat oral microbiome

Although HA5 and HA6 are efficient inhibitors of *S. mutans* biofilm and cariogenic activity [18], it is important to ensure that these compounds do not have any deleterious impact on the healthy oral microbial community. To understand how these compounds affect the residential bacterial community, we conducted an *in vivo* evaluation of both HA5 and HA6 and compared to the untreated and NaF-treated rats using a well-established gnotobiotic rat model of dental caries [57–61]. Treatment groups used in this study were inhibitor HA5 (100 μM), inhibitor HA6 (100 μM), and vehicle. A UA159 infection only group served as a negative control and a NaF (250 ppm) served as a positive control.

All rats from the experimental groups and from the control groups were colonized with *S. mutans* UA159. A 4-week treatment of infected gnotobiotic rats with HA5 or HA6 resulted in significant reductions in buccal caries scores from the enamel (E) and dentinal slight (Ds), dentinal medium (Dm), and dentinal extensive (Dx) compared to control groups (Table 1). Similar reductions were observed in sulcal and proximal caries scores (Table 2). The effect of the treatment on dentinal moderate (Dm) and dentinal extensive (Dx) scores in the proximal area were not recorded as there were no observable caries lesions in both control and the treated groups. The observed reductions in caries scores by HA5 or HA6 were slightly lower than the positive control NaF treatment. However, it should be noted that the concentration of NaF

Table 1
Effect of HA5 or HA6 treatment on *S. mutans* UA159 induced buccal caries.

Treatment Group	Buccal Mean, Caries Scores, (± SEM)			
	E	Ds	Dm	Dx
UA159 infected and untreated	13.2 ± 0.4	9.2 ± 0.6	6.2 ± 0.7	3.6 ± 0.4
HA5 treated (100 μM)	7.8 ± 0.4	6.6 ± 0.5	3.6 ± 0.4	2.2 ± 0.7
HA6 treated (100 μM)	8.2 ± 0.7	6.8 ± 0.5	4.0 ± 0.7	1.2 ± 0.5
NaF treated (250 ppm)	6.2 ± 0.9	3.2 ± 0.9	1.6 ± 0.5	0.4 ± 0.2

Enamel (E); Dentinal slight (Ds); Dentinal moderate (Dm); Dentinal extensive (Dx), n = 5.

Table 2
Effect of HA5 or HA6 treatment on *S. mutans* UA159 induced sulcal and proximal caries.

Treatment, Group	Mean Caries Scores (± SEM) Sulcal Mean Caries Scores, (± SEM)				Proximal Mean Caries Scores, (± SEM)	
	E	Ds	Dm	Dx	E	Ds
UA159 infected and untreated	25.8 ± 1.2	18.8 ± 1.3	12.8 ± 0.7	6.6 ± 0.3	8.0 ± 0.0	5.8 ± 0.7
HA5 treated (100 μM)	16.4 ± 2.2	11.2 ± 0.6	4.6 ± 0.2	1.0 ± 0.3	1.0 ± 0.3	0.0 ± 0.0
HA6 treated (100 μM)	14.6 ± 0.9	11.2 ± 0.7	6.4 ± 0.4	1.6 ± 0.4	1.2 ± 0.8	0.0 ± 0.0
NaF treated (250 ppm)	15.2 ± 0.7	10.4 ± 0.5	5.4 ± 0.4	1.6 ± 0.5	0.0 ± 0.0	0.0 ± 0.0

Enamel (E); Dentinal slight (Ds); Dentinal moderate (Dm); Dentinal extensive (Dx), n = 5.

(250 ppm = 5.95 mM) is about 59-fold higher than the inhibitor treatment dose of 100 μM. In addition, the rats treated with the compound HA5 or HA6 did not experience significant weight loss over the course of the study, suggesting that the compounds are non-toxic (Table 3). Furthermore, HA5 or HA6 treatment did not affect bacterial colonization significantly compared to control group (Table 3).

During this study, rat oral microbiome samples were collected from individual rats (n = 5) at the following time points: before the experiment (Native), after inoculation of *S. mutans* and the start of a caries-promoting diet (Sm+CPD), after two weeks of treatment with the compound (2-week), and at the end of the study (END). The microbiota between the groups at different time points was analyzed for oral bacterial composition and abundance. Oral swabs collected before and after interventions with these compounds were analyzed using the 16 s rRNA gene sequencing method. Both 'within' (alpha diversity) and 'between' (beta diversity) sample diversities were calculated over time for each treatment group using MicrobiomeAnalyst 2.0 [55].

The major phyla detected in the study are Firmicutes, Proteobacteria, Bacteroides, Actinobacteria, Verrucomicrobia, Epsilonbacteraeota, Tenericutes, Cyanobacteria, and Spirochaetes. Phylum level comparison of oral microbiome samples from initial infection of *S. mutans* after 2-week of treatment and 4-week treatment showed that the phylum Firmicutes dominated the native microbiome and to a lesser extent by phyla Proteobacteria and Bacteroides. Treatment with the compounds HA5 or HA6 did not perturb the overall rat oral microbiome at phylum levels significantly (Fig. 4A). Each color represents 1 phylum, and the length of the bar reflects relative abundance. The results were similar to the NaF treatment and the control: infected untreated animals.

Table 3
Effect of HA5 or HA6 treatment on *S. mutans* UA159 CFU and the body weight of the treated animals.

Treatment Group	CFU/mL (x10^5)		Animals	
	MS	BAP	Weight (g)	Number
UA159 infected and untreated	2.3 ± 1.2	3.3 ± 2.0	161 ± 12	5
HA5 treated (100 μM)	2.2 ± 0.8	3.9 ± 1.4	156 ± 16	5
HA6 treated (100 μM)	1.3 ± 0.4	1.9 ± 0.5	165 ± 13	5
NaF treated (250 ppm)	1.6 ± 0.6	2.8 ± 0.7	145 ± 12	5

Mitis-Salivarius agar (MS); Blood agar plate (BAP)

The family level comparison within the major phylum, Firmicutes, from the initial infection of *S. mutans* to after 4-week of treatment was carried out. The major families detected within the phylum Firmicutes throughout the study are Lachnospiraceae, Ruminococcaceae, Lactobacillaceae, Erysipelotrichaceae, and Streptococcaceae. Each color represents 1 family, and the length of bar reflects relative abundance (Fig. 4B). The results suggested that the Lachnospiraceae family dominated in the native microbiome and, to a lesser extent by families Ruminococcaceae and Lactobacillaceae and the treatment with compounds HA5 or HA6 did not perturb the overall rat oral microbiome significantly within this phylum (Fig. 4B). However, an increase in the abundance of the Streptococcaceae family was observed during the second week of the study for untreated and fluoride treated groups. This increase was not sustained till the end of the study as the week 4 abundance of Streptococcaceae composition was found to be similar to the native group suggesting that the observed increase in abundance during week 2 was likely an experimental artifact. Overall, the results of compound treatment were similar to NaF treatment and the control: infected untreated animals.

A comparative analysis plots of alpha-diversity of all animals in groups over time, Native (black) and END (gray) are presented in Fig. 4C. As in untreated control groups, the treated groups also maintained an increasing trend in the alpha diversity at the end of the treatment. Both compounds HA5 and HA6 maintained the beta diversity without any significant deviations (PERMANOVA, P-value > 0.05) from the native community (Fig. 4D). None of the groups showed any change in the community after Sm + CPD treatment, except the NaF-treated group (PERMANOVA, P-value > 0.001), where the community was shifted, and the samples were clustered separately. However, after 2 weeks of treatment, it shifted closer to the native state. Similar to what we observed in the untreated group, the intervention for a total of 4 weeks with these compounds did not show any shift in the oral bacterial community, indicating the harmless nature of these compounds towards other commensal bacteria in the oral cavity.

3.5. Design of pH-responsive polymersome vesicles

Spherical block copolymer vesicles that allow the encapsulation of both hydrophilic and hydrophobic drugs were designed and synthesized. The hollow block copolymer vesicles were assembled from poly(N-vinylpyrrolidone)$_8$-*block*-poly(dimethylsiloxane)$_{64}$-*block*-poly(N-vinylpyrrolidone)$_8$ (PVPON$_8$-PDMS$_{64}$-PVPON$_8$) triblock copolymer into ~30 nm vesicles using a nanoprecipitation method [62,63]. The block copolymer was synthesized by reversible addition-fragmentation chain transfer (RAFT) polymerization of *N*-vinylpyrrolidone (VPON) from PDMS macroinitiator as we have previously reported (Fig. 5A) [64]. The molecular weight of the purified copolymer was determined by ^{1}H NMR (Fig. 5B) and was found to be M_n = 7070 g/mol (See Materials and Methods Section for details). Due to the presence of acid labile ester linkages between PDMS and PVPON blocks in the triblock copolymer, the assembled polymersome vesicles are degraded when pH is lowered to < 4, as we demonstrated earlier [62,65].

3.6. Polymersome encapsulation of compounds HA5 or HA6

TEM analysis of the empty polymersomes (Fig. 5C) demonstrated the presence of intact spherical vesicles. The average size of the dry vesicles was determined across 100 measurements and found to be 30.1 + /- 2.7 nm, which agrees with the DLS size data from the same vesicle

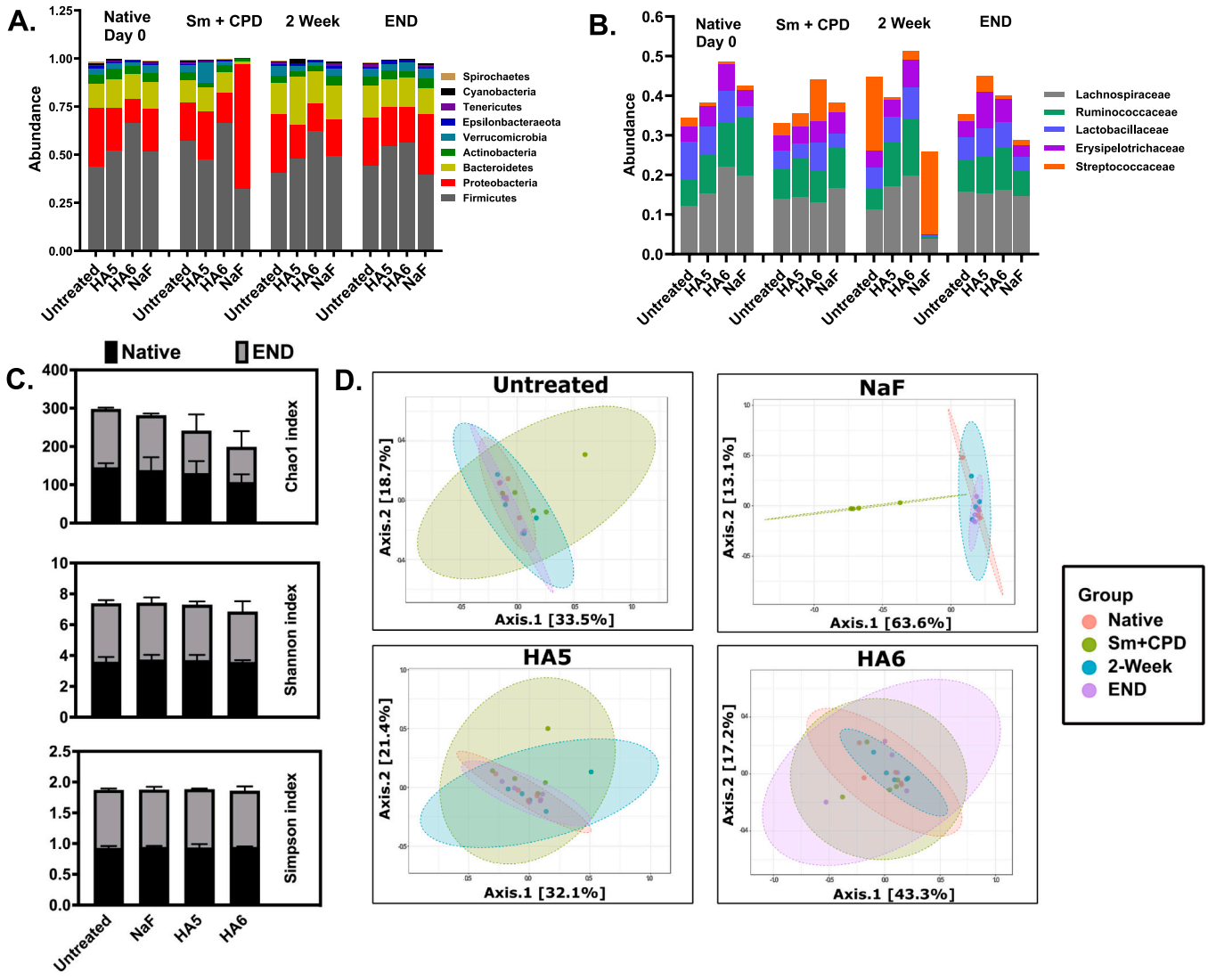

Fig. 4. Compounds HA5 and HA6 do not perturb oral microbiome significantly. Oral microbiome samples were obtained from individual rats at the following time points: before the experiment (Native), after inoculation of *S. mutans* and the start of a caries-promoting diet (Sm+CPD), after two weeks of treatment with the compounds (2-week), and at the end of the study (END). The microbiota between groups at different time points were analyzed for diversity and composition. A) Phyla composition in all groups. Each color represents 1 phylum, and the length of the bar reflects relative abundance. The major phyla detected throughout the study were Firmicutes, Proteobacteria, Bacteroides, Actinobacteria, Verrucomicrobia, Epsilonbacteraeota, Tenericutes, Cyanobacteria, and Spirochaetes. $n = 5$ per group. B) Family-level composition within phylum Firmicutes. The major families detected within the phylum are Lachnospiraceae, Ruminococcaceae, Lactobacillaceae, Erysipelotrichaceae, and Streptococcaceae, $n = 5$. C) Alpha diversity of the oral bacterial community structure at the genus level of each treatment group. Three diversity indices: Chao-1, Shannon, and Simpson were calculated, before (Native) and after (END) the treatment interventions and compared against the untreated group. $n = 5$. D) Beta diversity (Bray-Curtis index) of the oral bacterial community structure at the genus level for each treatment group is represented by the principal coordinates analysis (PCoA) plots where the samples were clustered (ellipses) based on the time points as depicted in the color legend: native (red), Sm+CPD (green), 2-week (blue) and END (purple). Each dot represents 1 rat, $n = 5$.

solution (Fig. 5D). For encapsulation of HA5 and HA6 into the polymeric vesicles, the $PVPON_8$-$PDMS_{64}$-$PVPON_8$ triblock copolymer solution in ethanol (5.0 mg/mL; 1 mL) was added dropwise to 4.0 mL of HA5 (0.625 mg/mL), or HA6 (0.625 mg/mL), solution in DI water at room temperature and left stirring for 2 h. The hydrodynamic sizes of purified PEHA5 and PEHA6 were measured using a Nano-ZS Zetasizer (Malvern Pananalytical) equipped with a He–Ne laser (663 nm) at 25 °C. The average hydrodynamic diameters were measured to be 33 ± 10 nm for empty vesicles (Fig. 5D) and 33 ± 11 nm and 28 ± 9 nm for PEHA5 and PEHA6, respectively (Fig. 5D). The concentration of encapsulated drug was calculated using UV–visible spectroscopy using calibration curves for HA5 (λ_{max} =444 nm) and HA6 (λ_{max} =412 nm) and was found to be 0.045 mg/mL for HA5 and 0.035 mg/mL for HA6. (Fig. 5E).

3.7. Biofilm and growth inhibitory activities of PEHA5

Prior to *in vivo* evaluations, the biofilm inhibitory activities of PEHA5 were investigated. PEHA5 inhibited *S. mutans* biofilm in a dose-dependent manner with an IC_{50} value of 12.04 ± 1.51 μM (Fig. 6A). Staining of the bacterial cells within biofilms with Syto-9 showed significant reduction in biofilms at 10 μM and a complete inhibition at 20 μM of PEHA5 (Fig. 6E-I). The presence of glucans, which were stained with Cascade Blue-dextran conjugated dye, was significantly reduced at 10 μM and no glucan formation was evident at 20 μM of PEHA5 (Fig. 6E-II). In addition, propidium iodide was used to determine the presence of eDNA in *S. mutans* biofilms. Again, there was a noticeable reduction of eDNA at 10 μM and almost complete absence of eDNA at 20 μM of PEHA5 (Fig. 6E-III). These findings reaffirm that PEHA5

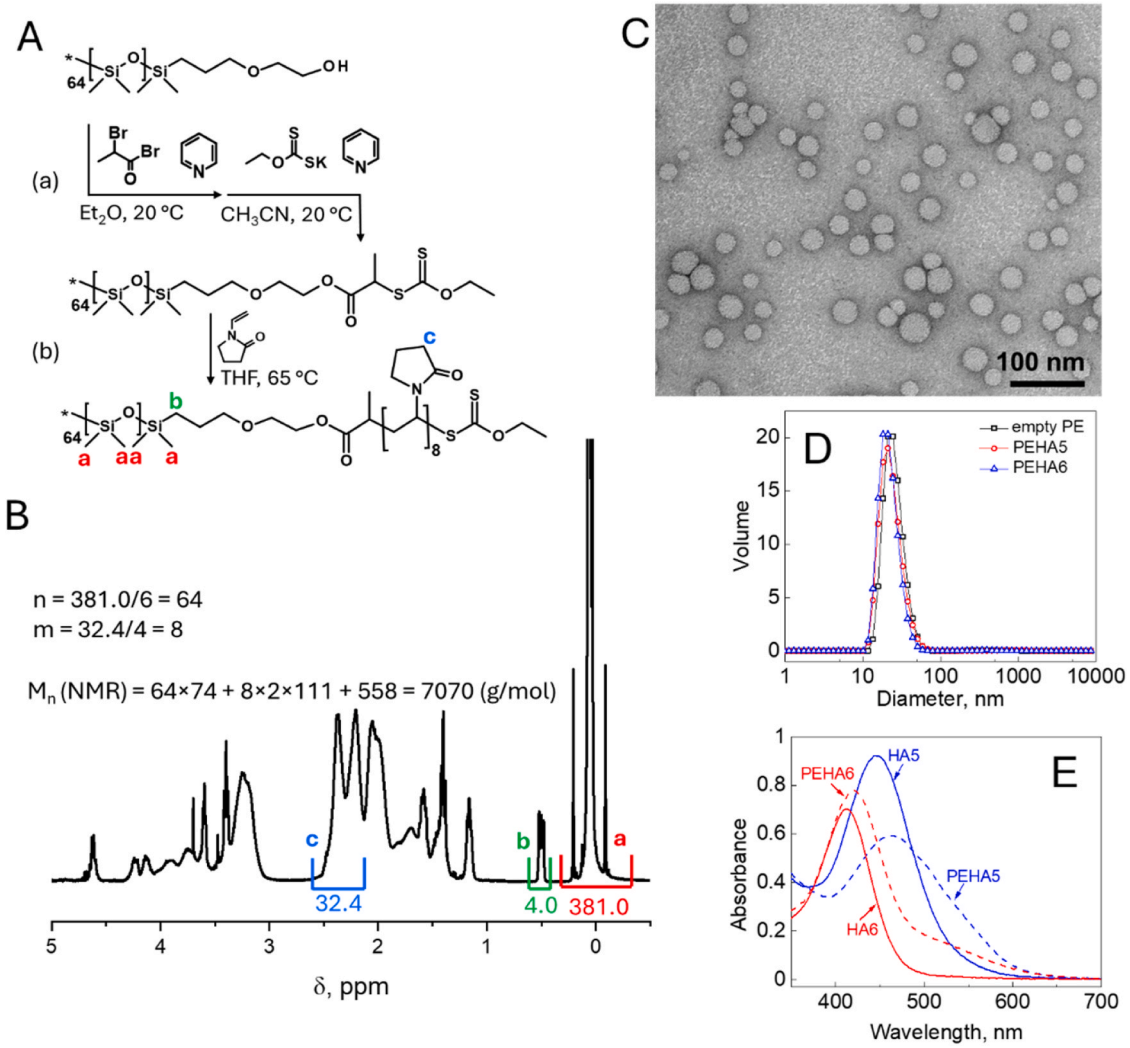

Fig. 5. A) Synthesis of $PVPON_8$-$PDMS_{64}$-$PVPON_8$ triblock copolymer by RAFT copolymerization (*a mirrored chemical structure). B) ^1H NMR spectrum of $PVPON_8$-$PDMS_{64}$-$PVPON_8$ triblock copolymer. C) Representative TEM image of $PVPON_8$-$PDMS_{64}$-$PVPON_8$ copolymer vesicles dried on a formvar-coated Cu grid (mesh 200). D) Hydrodynamic size (diameter, nm) of empty polymersome and PEHA5 and PEHA6 as measured by DLS. **E)** UV–visible spectra of HA5 and HA6 (solid lines) and PEHA5 and PEHA6 (dotted lines) in water.

exhibited *S. mutans* biofilm inhibitory activities similar to what is reported for unencapsulated compound HA5 [18]. The effects of unloaded polymersome vesicles on *S. mutans* biofilm were compared with the control (1 % DMSO) and the biofilm inhibitory activities of PEHA5 and HA5 at a single dose of 50 μM concentration. Clearly, empty polymersome vesicles did not inhibit the biofilm as compared to 80 % inhibition by PEHA5 and 95 % inhibition by HA5 (Fig. 6B). The planktonic growth of *S. mutans* was not affected by PEHA5 at the range of doses of 5 μM - 50 μM (Fig. 6C). In addition, the effect of PEHA5 on the planktonic growth of two commensal Streptococci, *S. gordonii* and *S. Sanguinis* were compared with the control (1 % DMSO) and HA5 at a single treatment dose of 50 μM. Compared to control, PEHA5 slightly inhibited the growth of *S. gordonii* and *S. sanguinis* at this dose, but the effects were minimal (Fig. 6D).

3.8. Biofilm and growth inhibitory activities of PEHA6

The biofilm inhibitory activities of PEHA6 were investigated**.** PEHA6 inhibited *S. mutans* biofilm in a dose-dependent manner with an IC_{50} value of 8.09 ± 2.92 μM (Fig. 7A). Staining of the bacterial cells within biofilms with Syto-9 showed significant reduction in biofilms at 10 μM and a complete inhibition at 20 μM of PEHA6 (Fig. 7E-I). The presence of glucans, which were stained with Cascade Blue-dextran conjugated dye, was significantly reduced at 10 μM and no glucan formation was evident at 20 μM of PEHA6 (Fig. 7E-II). In addition, propidium iodide was used to determine the presence of eDNA in *S. mutans* biofilms. Again, there was a substantial decrease in eDNA at 10 μM and almost complete absence of eDNA at 20 μM of PEHA6 (Fig. 7E-III). These findings suggest that PEHA6 demonstrated *S. mutans* biofilm inhibitory activities comparable to unencapsulated compound HA6. The effects of PEHA6 on *S. mutans* biofilm were compared with the control (1 % DMSO) and the biofilm inhibitory activities of HA5 and HA6 side by side at a single dose, 50 μM concentration. Clearly, PEHA6 inhibited 95 % of the biofilm closely resembling the efficacy of HA6, with HA5 showing an 85 % inhibition of biofilm (Fig. 7B). The planktonic growth of *S. mutans* was not affected by PEHA6 at the range of doses of 5 μM - 50 μM (Fig. 7C). In addition, the effect of PEHA6 on the planktonic growth of *S. mutans* was compared with HA5, HA6 at 50 μM. Compared to control, PEHA6 and HA6 inhibited the planktonic growth slightly while HA5 did not inhibit the growth significantly at this dose (Fig. 7D).

3.9. Reduction of S. mutans virulence in vivo by PEHA5

The effect of PEHA5 on *S. mutans* colonization and virulence was

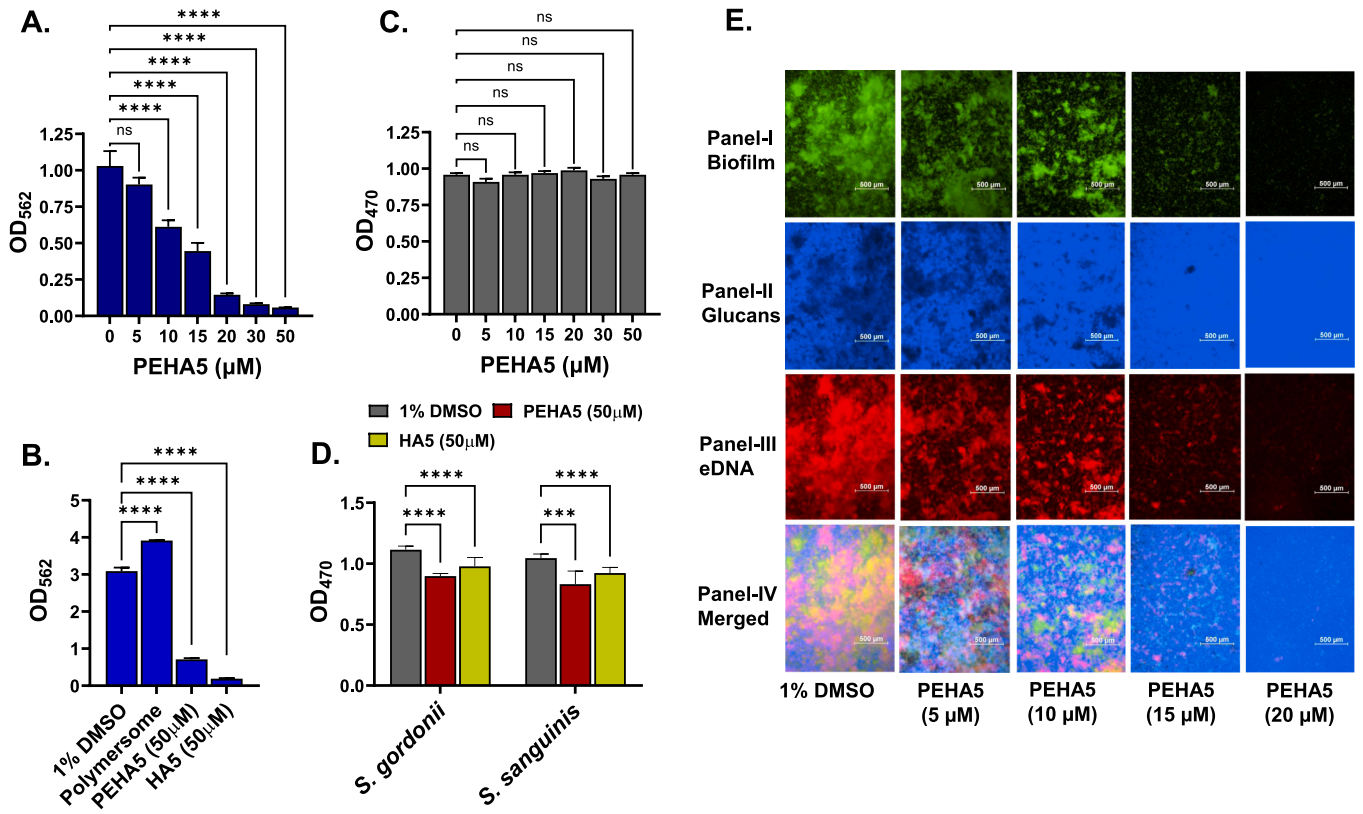

Fig. 6. Biofilm and growth inhibitory activities of PEHA5. A) *S. mutans* UA159 were co-incubated with various concentrations of PEHA5, and biofilm formation was measured at OD_{562} using the crystal violet protocol. B) *S. mutans* UA159 were co-incubated with empty polymersome vesicles, 50 μM of HA5 or PEHA5 and the biofilm formation compared to control (1 % DMSO) was measured at OD_{562} using the crystal violet protocol. C) *S. mutans* UA159 were co-incubated with various concentrations of PEHA5, and the planktonic growth was measured at OD_{470}. D) *S. mutans* UA159 and two bacterial commensal species *S. sanguinis* SK36 and *S. gordonii* DL1 co-incubated with PEHA5 or HA5 at 50 μM and their planktonic growth was measured at OD_{470}. E) Representative fluorescence microscopy images of UA159 biofilms after 16 h of treatment with various concentrations of PEHA5. Bacterial cells were stained with Syto-9 (green, panel-I); glucans were stained with Cascade Blue–dextran conjugated dye (blue, panel-II); eDNA was stained with propidium iodide (red, panel-III), and a merged image of all three staining images (panel-IV).

compared side-by-side with HA5 using a well-established gnotobiotic rat model of dental caries [57–61]. A (vehicle + infection only) group was included as a negative control. All rats from the experimental groups and from the control group were colonized with *S. mutans* UA159. A 4-week treatment of *S. mutans* UA159 infected gnotobiotic rats with 100 μM of PEHA5 or HA5 resulted in significant reductions in buccal caries scores for enamel (E), dentinal slight (Ds), dentinal moderate (Dm), and dentinal extensive (Dx) lesions compared to control groups (Table 4). Similar reductions in caries scores were also observed in sulcal caries scores and proximal caries scores (Table 5). We were unable to record the effect of the treatment on dentinal moderate (Dm) and dentinal extensive (Dx) scores in the proximal area due to the absence of dentinal lesions in the control and treated groups. The observed reductions in caries scores by PEHA5 were comparable with HA5, with the PEHA5 displaying slightly better *in vivo* activity, possibly due to the slow pH-dependent release of the drug from PEHA5 over the treatment period. In addition, the rats treated with PEHA5 or HA5 did not experience any weight loss over the course of the study in comparison with the control group, suggesting the non-toxic nature of the material and the compound (Table 6). Furthermore, PEHA5 or HA5 treatment did not affect bacterial colonization significantly (Table 6).

4. Discussion

Human oral cavity maintains a healthy pH of 6.0 – 7.5 in the oral cavity [19,20] under physiological conditions controlled by buffer systems [21,22]. Under pathogenic conditions, the dental biofilm ferments the dietary carbohydrates to produce lactic acid leading to a drop in pH to less than 5.5, which is harmful to the tooth enamel and dentin [21–24]. Therefore, dental caries treatment would tremendously benefit from an antibiofilm agent that is delivered on the tooth surface in a pH-responsive manner. The goal of this study is to encapsulate the biofilm inhibitors HA5 and HA6 in pH-responsive polymersome vesicles and explore their potential for pH-responsive treatment for dental caries.

Towards this goal, we have synthesized two biofilm inhibitors HA5 and HA6 using the synthetic protocols reported from our lab recently [18]. The evaluation of Gtf inhibition, biofilm inhibition and growth inhibition activities of the compound HA5 has already been reported in our prior publication [18]. Additional *in vitro* and *in vivo* evaluations of HA6 to ensure its activity and suitability for polymersome encapsulation showed that the compound HA6 selectively inhibited *S. mutans* biofilms with an IC_{50} value of 18.92 ± 0.39 μM without affecting the planktonic growth of *S. mutans* at its biofilm inhibiting doses. Its selectivity towards biofilm inhibition and potential for preserving oral microbiome is indicated by its lack of inhibition of the planktonic growth of two representative oral commensal species, *S. sanguinis* and *S. gordonii* at its biofilm inhibiting dose. In addition, the compound HA6 did not significantly reduce the biofilms of the commensal species *S. gordonii* and *S. sanguinis* at 25 μM. The compound HA6 inhibited *S. mutans* Gtfs and glucan production with and the IC_{50} value of 8.90 ± 0.22 μM. The Gtf binding of HA6 was further supported by SeeSAR docking studies using the reported GtfB+HA5 complex crystal structure [18]. The results of this study suggest that the inhibitor HA6 binds within GtfB active site

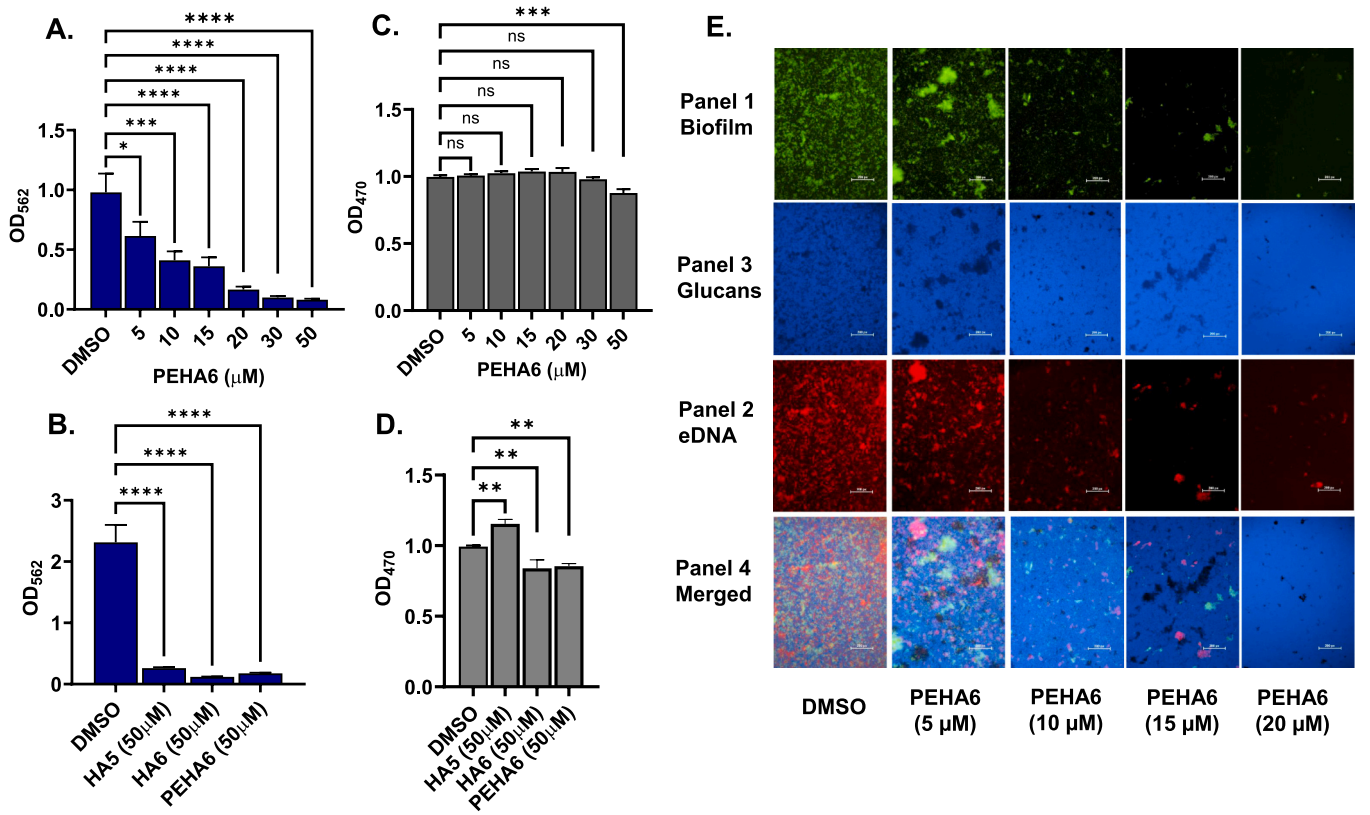

Fig. 7. Biofilm and growth inhibitory activities of PEHA6. A) *S. mutans* UA159 were co-incubated with various concentrations of PEHA6, and biofilm formation was measured at OD_{562} using the crystal violet protocol. B) *S. mutans* UA159 were co-incubated with 50 μM of HA5, HA6, or PEHA6 and the biofilm formation compared to control (1 % DMSO) was measured at OD_{562} using the crystal violet protocol. C) *S. mutans* UA159 were co-incubated with various concentrations of PEHA6, and planktonic growth was measured at OD_{470}. D) *S. mutans* UA159 co-incubated with HA5, HA6 or PEHA6 at 50 μM and their planktonic growth was measured at OD_{470}. E) Representative fluorescence microscopy images of UA159 biofilms after 16 h of treatment with various concentrations of PEHA6. Bacterial cells were stained with Syto-9 (green, panel-I); glucans were stained with Cascade Blue–dextran conjugated dye (blue, panel-II); eDNA was stained with propidium iodide (red, panel-III), and a merged image of all three staining images (panel-IV).

Table 4
Effect of PEHA5 or HA5 treatment on *S. mutans* UA159 induced buccal caries.

Treatment, Group	Buccal Mean, Caries Scores, (± SEM)			
	E	Ds	Dm	Dx
UA159 infected and untreated	13.8 ± 0.9	11.4 ± 0.5	8.2 ± 0.4	5.6 ± 0.7
PEHA5 treated (100 μM)	7.4 ± 0.6	5.4 ± 0.7	4.0 ± 0.6	1.4 ± 0.9
HA5 treated (100 μM)	9.0 ± 0.6	6.4 ± 1.0	2.8 ± 0.5	1.4 ± 0.4

Enamel (E); Dentinal slight (Ds); Dentinal moderate (Dm); Dentinal extensive (Dx)

Table 5
Effect of PEHA5 or HA5 treatment on *S. mutans* UA159 induced sulcal and proximal caries.

Treatment, Group	Mean Caries Scores (± SEM), Sulcal Mean Caries Scores, (± SEM)				Proximal Mean Caries Scores, (± SEM)	
	E	Ds	Dm	Dx	E	Ds
UA159 infected and untreated	24.2 ± 0.9	18.4 ± 0.7	13.4 ± 0.9	7.0 ± 0.3	6.8 ± 0.8	4.6 ± 1.0
PEHA5 treated (100 μM)	16.0 ± 0.8	12.6 ± 0.7	6.6 ± 0.5	2.6 ± 0.5	4.0 ± 1.1	1.6 ± 1.0
HA5 treated (100 μM)	20.6 ± 0.8	15.0 ± 0.9	9.4 ± 0.5	4.8 ± 0.9	5.2 ± 0.5	3.4 ± 0.6

Enamel (E); Dentinal slight (Ds); Dentinal moderate (Dm); Dentinal extensive (Dx)

similar to HA5 and revealed several key interactions of HA6 with the active site resides.

To understand how these compounds affect the residential bacterial community, we conducted an *in vivo* evaluation of both inhibitors and compared their activity to the untreated rats and NaF-treated rats using a well-established gnotobiotic rat model of dental caries [57–61]. A 4-week treatment of infected gnotobiotic rats with 100 μM of HA5 or HA6 resulted in significant reductions in buccal caries scores from the enamel (E) and dentinal slight (Ds), dentinal medium (Dm), and dentinal extensive (Dx) compared to control groups. Similar reductions were observed in sulcal and proximal caries scores. The observed reductions in caries scores by HA5 or HA6 were slightly lower than the positive control NaF treatment. However, it should be noted that the concentration of NaF (250 ppm = 5.95 mM) is about 59-fold higher than the inhibitor treatment dose of 100 μM.

During this study, the rat oral microbiome samples were collected from individual rats (n = 5) at the following time points and the microbiota between the groups at different time points was analyzed for oral bacterial composition and abundance. The family level comparison within the major phylum, Firmicutes suggested that the treatment with compounds HA5 or HA6 did not perturb the rat oral microbiome significantly within this phylum. An increase in the abundance of the Streptococcaceae family was observed during the second week of the study for the untreated and fluoride treated groups. However, this increase was not sustained till the end of the study as the week 4 abundance of Streptococcaceae composition was found to be similar to the

Table 6
Effect of PEHA5 or HA5 treatment on *S. mutans* UA159 CFU and the body weight of the treated animals.

Group	CFU/mL (x10^5)		Animals	
	MS	BAP	Weight (g)	Number (n)
UA159 infected and untreated	3.2 ± 0.6	3.9 ± 0.4	140 ± 9	5
PEHA5 treated (100 μM)	1.4 ± 0.4	3.4 ± 0.9	149 ± 16	5
HA5 treated (100 μM)	5.5 ± 2.6	5.2 ± 1.4	145 ± 14	5

Mitis-Salivarius agar (MS); Blood agar plate (BAP)

native group suggesting that the observed increase in abundance during week 2 was likely an experimental artifact. Overall, the results of the compound treatment were similar to NaF treatment and the control untreated animals. The principal component analysis plots of alpha-diversity of all animals in groups over time showed that none of the groups showed any change in the community after Sm + CPD treatment, except the NaF-treated group (PERMANOVA, P-value > 0.001), where the community was shifted, and the samples were clustered separately. However, after 2 weeks of treatment, it shifted closer to the native state. Similar to what we observed in the untreated group, the intervention for a total of 4 weeks with the compounds HA5 or HA6 did not show any shift in the oral bacterial community, indicating the harmless nature of these compounds towards other commensal bacteria in the oral cavity.

In similar reported studies, killing and elimination of *S. mutans* by synthetic antimicrobial peptide C16G2 in an *in vitro* oral biofilm model in saliva nonspecifically eliminated noncariogenic species, leading to a drastic shift of the structure of the microbiota [66]. A novel small molecule 3F1 significantly reduced caries scores *in vivo* without affecting the rat oral microbiome, however, the underlying mechanism of the dispersion agent is unknown [67]. Our microbiome analysis data suggests that the novel small molecules HA5 and HA6 significantly reduced the caries scores *in vivo* without affecting the rat oral microbiome like 3F1, and the inhibition of *S. mutans* biofilm is sufficient to decrease the incidence of dental caries. Any type of dysbiosis in the oral microbiota may favor the dental caries promoting organisms and result in adverse effects. Thus, targeting the bacterial species that promote dental carries without any major perturbation to normal healthy microbiota has greater implications in maintaining dental health.

After conducting the *in vitro* and *in vivo* evaluations of the compounds HA5 and HA6, they were encapsulated into spherical block copolymer vesicles to generate polymersome encapsulated drugs PEHA5 and PEHA6 and their biofilm and growth inhibitory activities were evaluated in comparison with empty polymersome vesicles and unencapsulated drugs. Clearly, empty polymersome vesicles did not inhibit the biofilm as compared to 80 % inhibition by PEHA5 and 95 % inhibition by HA5 at 50 μM. The planktonic growth of *S. mutans* was not affected by PEHA5 up to 50 μM. In addition, the study on commensal species indicated that PEHA5 slightly inhibited the growth of *S. gordonii* and *S. sanguinis* at this dose, but the effects were minimal. Similarly, PEHA6 also inhibited *S. mutans* biofilm by 95 % closely resembling the efficacy of HA6. The planktonic growth of *S. mutans* was not affected by PEHA6 at the treatment dose of 50 μM. Again, the lack of inhibition of planktonic growth of *S. mutans* and commensal species by PEHA5 and PEHA6 indicates their potential to preserve oral microbiome during treatment.

Finally, the effect of PEHA5 on *S. mutans* colonization and virulence was compared side-by-side with HA5 using a well-established gnotobiotic rat model of dental caries [57–61]. PEHA5 was found to be effective in reducing the caries lesions without affecting bacterial colonization after a 4-week treatment. The observed reductions in buccal, sulcal and proximal caries scores by PEHA5 were comparable with HA5, with the PEHA5 displaying slightly better *in vivo* efficacy, possibly due to the slow pH-dependent release of the drug from PEHA5 over the treatment period. In addition, the rats treated with PEHA5 did not experience any weight loss over the course of the study in comparison to the control group, suggesting the non-toxic nature of the material. Our data suggests that PEHA5 releases HA5 under the acidic conditions of the dental caries infected oral cavity and reduce the cariogenic activity. The reduction in caries scores produced by PEHA5 are comparable to that achieved by HA5 treatment alone.

Taken together, our data suggest that the compound HA5 and the polymersome encapsulated material, PEHA5 selectively targeted *S. mutans* virulence factors; Gtfs and Gtf- mediated biofilm formation, rather than a simple inhibition of bacterial growth and are very effective in reducing dental caries *in vivo*. Overall, the results of our study suggest that the *S. mutans* biofilm-specific therapy using HA5, HA6, or the polymersome encapsulated materials reported here is a viable approach for preventing caries while preserving the oral microbiome.

5. Conclusions

The *in vivo* antivirulence activities and the potential of *S. mutans* biofilm inhibitors HA5 or HA6 to be a therapeutic that combines both species-specific selectivity towards *S. mutans* and preserves oral microbiome is demonstrated *in vivo* by characterizing the oral microbiome of the rats treated with these biofilm inhibitors. Phylum and family level comparison of the treatment groups from the time of initial infection with *S. mutans* to after 2-week and 4-week treatment with HA5 or HA6 showed selective control of *S. mutans* by the inhibitors without perturbing the overall rat oral microbiome significantly. Both inhibitors HA5 and HA6 were encapsulated into pH-responsive block copolymer vesicles to generate a polymersome-encapsulated biofilm inhibitors, PEHA5 and PEHA6 respectively and their biofilm and growth inhibitory activities against *S. mutans* and representative strains of oral commensal Streptococci have been assessed. A 4-week treatment of *S. mutans* UA159 infected gnotobiotic rats with 100 μM PEHA5 resulted in significant reductions in buccal, sulcal, and proximal dental caries scores compared to untreated control groups. These outcomes were comparable to those observed with 100 μM of HA5 treatment. Overall, our data suggests that the *S. mutans* biofilm-specific therapy using HA5, HA6, or the polymersome encapsulated materials reported here is a viable approach for preventing caries while preserving the oral microbiome.

Author contributions

Conceived the idea and designed the experiments: SEV, EK, HW, and SMM; Performed the experiments: PA, VK, PP, SN, MD, and GH. Analyzed data: LA, Drafted and finalized the manuscript, SEV, PA, VK, and EK.

Acknowledgements

The contents described in this report were supported by the National Institute of Dental and Craniofacial Research, National Institutes of Health grants R21DE028349 (Velu), R03DE025058 (Velu), R01DE022350 (Wu), and University of Alabama at Birmingham Microbiome Center Pilot Grant (Velu). This work was also supported by NSF DMR Award No. 2208831 (Kharlampieva). This material is in part based upon work supported under the IR/D Program by the National Science Foundation (Kharlampieva). Any opinion, findings, and conclusions or recommendations expressed in this material are those of the author(s) and do not necessarily reflect the views of the National Science Foundation.

Institutional animal care and use committee statement

All experimental protocols for animal study were approved by the University of Alabama at Birmingham Institutional Animal Care and Use Committee (protocol No: IACUC-20047). The methods were carried out

in accordance with the relevant guidelines and regulations.

Appendix

Contents: ^{1}H NMR and ^{13}C NMR spectra and spectral data of the compounds HA5 and HA6.

2- [(2,4,5-Trihydroxyphenyl)methylidene] -2,3-dihydro-1-benzofuran-3-one (HA5): 83 % yield, red solid; ^{1}H NMR (400 MHz, DMSO-d_6) δ: 9.91 (s, 1 H), 9.85 (s, 1 H), 8.72 (s, 1 H), 7.78–7.74 (m, 2 H), 7.61 (s, 1 H), 7.50 (d, 1 H, J = 8.5 Hz), 7.29 (t, 1 H, J = 7.5), 7.21 (s, 1 H), 6.44 (s, 1 H); ^{13}C NMR (100 MHz, DMSO-d_6) δ: 182.6, 164.5, 153.1, 150.7, 143.8, 139.0, 136.7, 124.0, 123.5, 121.7, 116.6, 113.0, 109.4, 108.6, and 103.1; HRMS calculated for $C_{15}H_{10}O_5$ 270.0528, found 270.0529.

2- [(3,4,5-Trihydroxyphenyl)methylidene] -2,3-dihydro-1-benzofuran-3-one (HA6): 86 % yield, greenish-yellow solid; ^{1}H NMR (400 MHz, DMSO- d_6) δ: 9.30 (brs, 1 H), 9.08 (brs, 1 H), 7.80–7.76 (m, 2 H), 7.50 (d, 1 H, J = 8.6 Hz), 7.30 (t, 1 H, J = 7.8 Hz), 7.03 (s, 2 H), 6.73 (s, 1 H); ^{13}C NMR (100 MHz, DMSO-d_6) δ: 183.0, 164.9, 146.2, 144.8, 137.2, 137.0, 124.2, 123.7, 122.0, 121.4, 114.5, 113.0, and 111.3; HRMS [M-H]$^{-}$ calculated for $C_{15}H_{10}O_5$ 269.0450, found 269.0445.

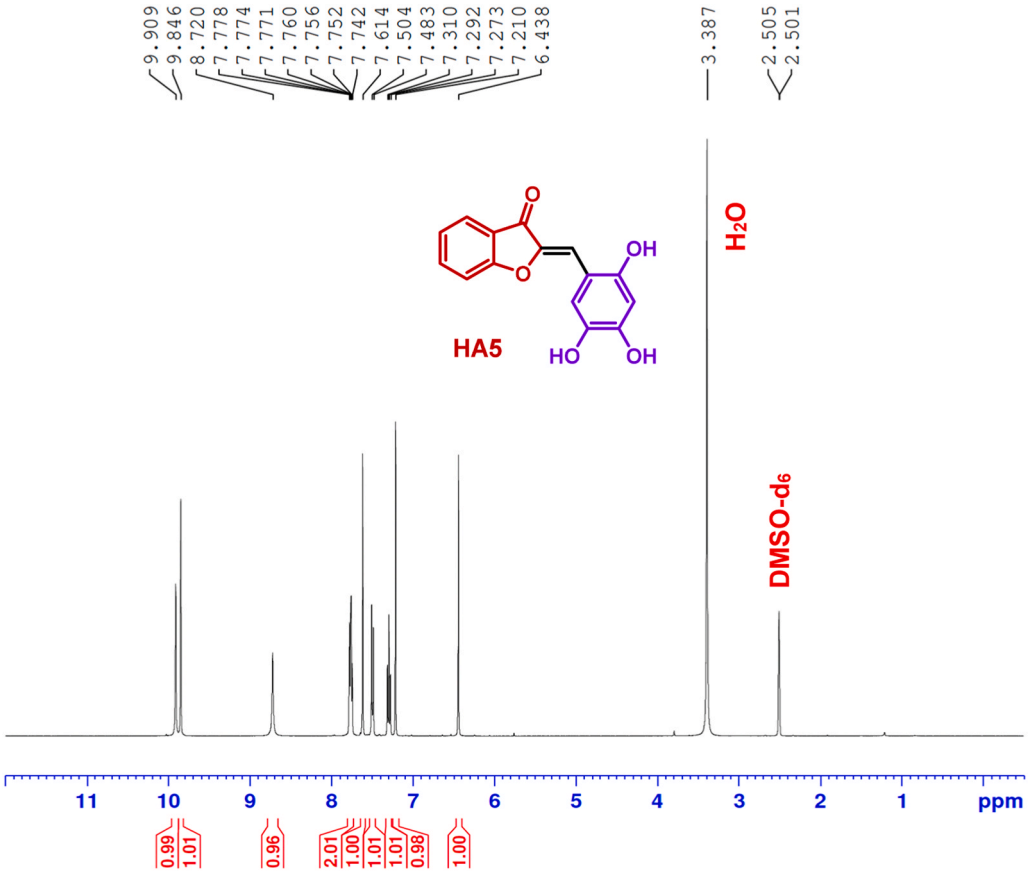

2-[(2,4,5-Trihydroxyphenyl)methylidene]-2,3-dihydro-1-benzofuran-3-one **(HA5)**.
^{1}H NMR (400 MHz, DMSO-d_6)

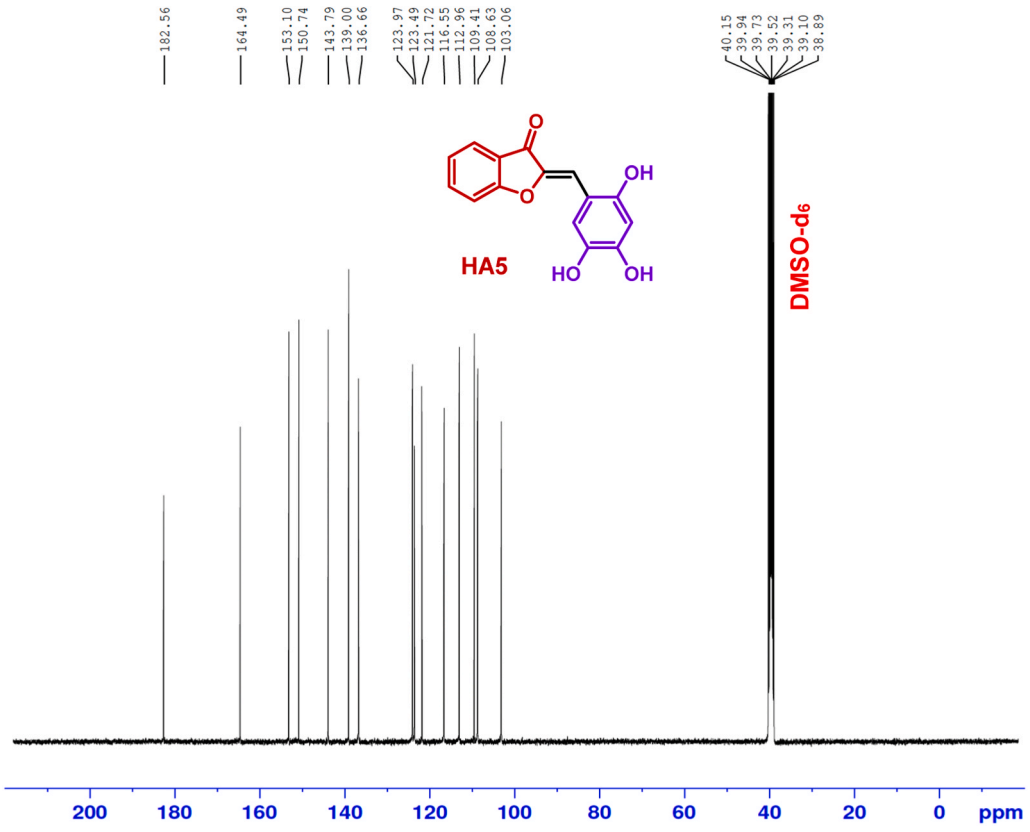

2-[(2,4,5-Trihydroxyphenyl)methylidene]-2,3-dihydro-1-benzofuran-3-one **(HA5)**.
^{13}C NMR (100 MHz, DMSO-d_6)

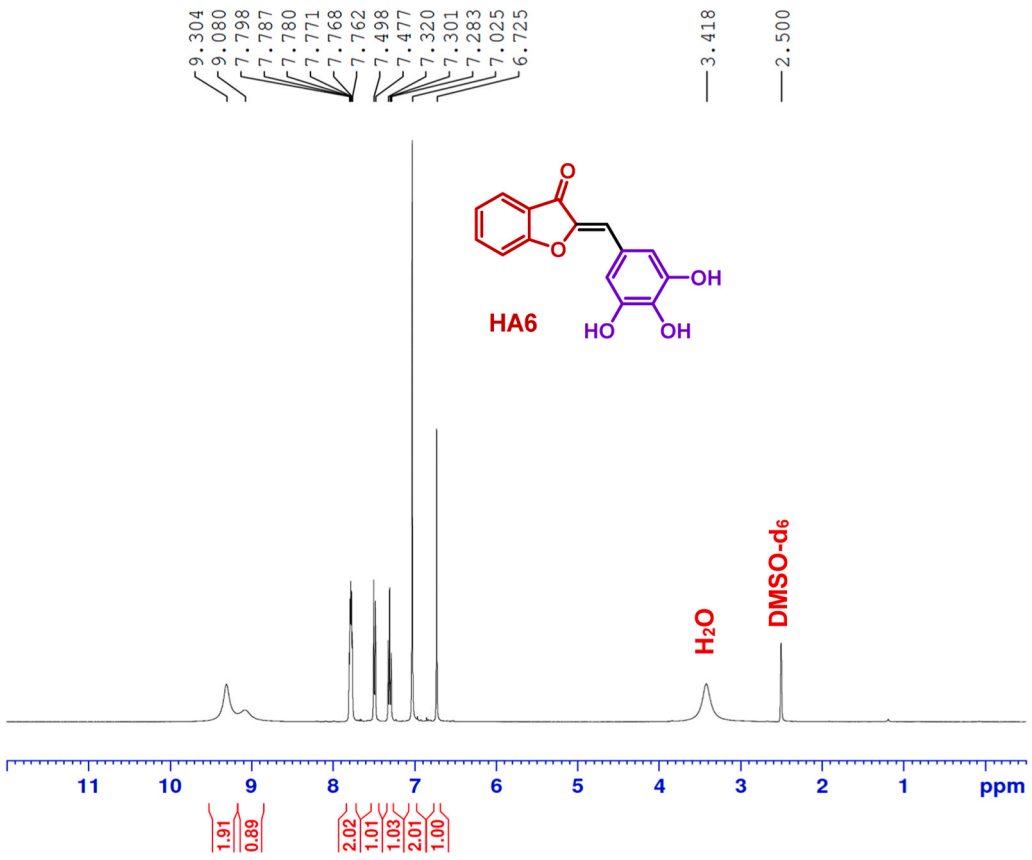

2-[(3,4,5-Trihydroxyphenyl)methylidene]-2,3-dihydro-1-benzofuran-3-one **(HA6)**.
^{1}H NMR (400 MHz, DMSO-d_6)

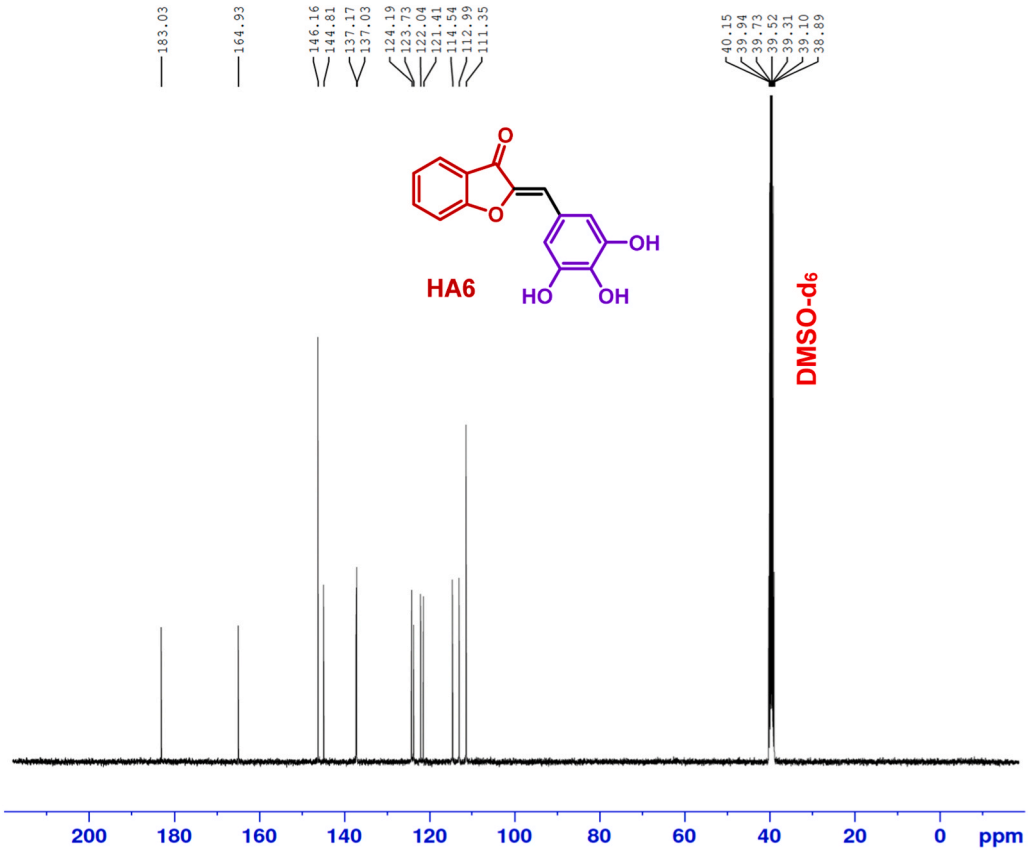

2-[(3,4,5-Trihydroxyphenyl)methylidene]-2,3-dihydro-1-benzofuran-3-one **(HA6)**.

^{13}C NMR (100 MHz, DMSO-d_6).

2.6 Fabrication of pH-responsive polymer vesicles.

2.6.1 Materials.

Hydroxyl terminated polydimethylsiloxane (PDMS, nominal average M_n ~ 5600, Sigma-Aldrich) was dried overnight in vacuum at 40 °C. Potassium ethyl xanthogenate (96 %, Sigma-Aldrich) and 2,2′-azobis(2-methylpropionitrile) (AIBN) (98 %, Sigma-Aldrich) were recrystallized before synthesis from methanol and acetone, respectively, and dried in vacuum at 20 °C. Acetonitrile (certified ACS grade), tetrahydrofuran (THF, HPLC grade), and 1-vinyl-2-pyrrolidone (VPON, 99 %) were purchased from Fisher Scientific and distilled before use. Diethyl ether (anhydrous), methanol, sodium hydroxide, hydrochloric acid, anhydrous sodium sulfate, and pyridine were purchased from Fisher Scientific and used as received. 2-Bromo-2-propionyl bromide (98 %, TCI) was stored under protective argon (Airgas) atmosphere and used as received.

2.6.2 Synthesis of $PVPON_8$-b-$PDMS_{64}$-b-$PVPON_8$ triblock copolymer.

For triblock copolymer synthesis, bis(hydroxyalkyl) poly(dimethylsiloxane) ($PDMS_{64}$) was first modified with 2-bromopropionyl bromide followed by potassium ethyl xanthogenate resulting in the PDMS macroinitiator. First, $PDMS_{64}$ terminated with dihydroxyl groups (10.0 g, 1.8 mmol) and pyridine (2.9 mL, 38 mmol) were mixed in a 250-mL round-bottom flask with 100 mL of anhydrous diethyl ester in an ice bath. A solution of 2-bromopropionyl bromide (3.0 mL, 24 mmol) in anhydrous diethyl ester (20 mL) was added dropwise to the mixture over 1 h. The solution was then allowed to warm to room temperature and was stirred for 24 h. The precipitate was separated by filtration and washed with 1.0 M HCl solution (3 times, 50 mL), 1.0 M NaOH solution (3 times, 50 mL), deionized (DI) water (4 times, 100 mL) and then dried with anhydrous sodium sulfate. Then, polymer solution was concentrated in a rotary evaporator and dried overnight under vacuum at room temperature. Next, dried polymer (9.8 g, 1.7 mmol) was added to acetonitrile (200 mL) in a 500-mL round-bottom flask and mixed with pyridine (2.9 mL, 38 mmol). Potassium ethyl xanthogenate (1.09 g, 6.8 mmol) dispersion in 20 mL of acetonitrile was added dropwise. The mixture was then stirred at room temperature overnight. After the precipitate was collected by filtration, the crude product was dissolved in 200 mL of diethyl ether. The organic solution was washed sufficiently with 1.0 M HCl solution (3 times, 50 mL), 1.0 M NaOH solution (3 times, 50 mL), and DI water (4 times, 100 mL) and then dried with anhydrous Na_2SO_4. Then, polymer solution was concentrated in a rotary evaporator and dried overnight under vacuum at room temperature. The final $PDMS_{64}$ macro-CTA was collected in 8.9 g and M_n was measured to be 7070 Da based on the ^{1}H NMR calculation of repeating units. The number-average molecular weight of $PDMS_{64}$-CTA was calculated from NMR analysis based on the ratio between the integrals at δ = 0–0.2 ppm (–SiC$\underline{H}_3$– protons in the PDMS block) and at δ = 0.6 ppm (–C$\underline{H}_2$O– protons from the end groups of PDMS). Then, PVPON blocks in $PVPON_8$-$PDMS_{64}$-$PVPON_8$ were synthesized by polymerization of N-vinylpyrrolidone (VPON) monomer by controlling the reaction time with a feed ratio of 1:1:95 by weight of $PDMS_{64}$ macroinitiator/AIBN/monomer. For that, macro-CTA (1.0 g, 0.19 mmol), VPON (2.0 g, 18 mmol), AIBN (33 mg, 0.21 mmol), and freshly distilled tetrahydrofuran (4 mL) were added in one 25 mL Schlenk flask (reactor) equipped with a magnetic stirring bar. The mixed solution was degassed by 3 freeze−pump−thaw cycles. The polymerization was initiated by immersion of the reaction mixture to the preheated oil bath at 65 °C. After 2 h, the reaction was immediately quenched in a liquid N_2. Then, the reaction mixture was diluted twice with methanol, transferred to dialysis tubes (MWCO = 500–1000 Da, Spectrum Laboratories), and dialyzed for 2 days in methanol. Then, polymer solution was concentrated in a rotary

evaporator and dried overnight under vacuum at room temperature. ^{1}H NMR spectra of the copolymer (15 mg mL^{-1} in $CDCl_3$) were collected on a Bruker 400 MHz NMR spectrometer. The molecular weight of PVPON-PDMS-PVPON was determined by ^{1}H NMR (600 MHz, Bruker). Average PVPON block length was calculated from ^{1}H NMR analysis based on the half of the ratio between the integrals at δ = 2.1–2.4 ppm (–C$\underline{H_2}$CO– protons from lactam ring of PVPON) and at δ = 0.6 ppm (–C$\underline{H_2}$O– protons from the end groups of PDMS). The monomer conversion was determined gravimetrically as the ratio of increase in the polymer weight to the initial monomer (VPON) content in the polymerization mixture, which was found to be 20.5 %.

4.6.3 Encapsulation of HA5 into polymer vesicles.

HA5 loaded polymersomes were prepared using a nanoprecipitation method. For that, 1.0 mL of the $PVPON_8$- $PDMS_{64}$- $PVPON_8$ triblock-copolymer solution in ethanol (5.0 mg/mL) was added dropwise to 4.0 mL of the 2.5 mg HA5 (or HA6) solution in DI water at room temperature and left under stirring for 2 h. Then, the obtained solution was dialysed in DI water for 48 h using a Float-a-Lyzer (MWCO 1000 Da, Fisher Scientific) to remove ethanol, followed by dialysis in DI water for 72 h using a Float-a-Lyzer (MWCO 100 kDa, Fisher Scientific) to remove an excess of the drug. The hydrodynamic size of empty and encapsulated polymersomes was measured using a Nano-ZS Zetasizer (Malvern Pananalytical) equipped with a He–Ne laser (663 nm) at 25 °C. Drug concentration was calculated using a NanoDrop One Microvolume UV-Vis spectrophotometer (Thermo Fisher).

References

[1] Marsh PD. Dental plaque as a microbial biofilm. Caries Res 2004;38:204–11.
[2] Vos T, Allen C, Arora M, Barber RM, Bhutta ZA, Brown A, et al. Global, regional, and national incidence, prevalence, and years lived with disability for 310 diseases and injuries, 1990-2015: a systematic analysis for the global burden of disease study 2015. Lancet 2016;388:1545–602.
[3] Hamada S, Slade HD. Biology, Immunology, and Cariogenicity of Streptococcus mutans. Microbiol Rev 1980;44:331–84.
[4] Loesche WJ. Role of streptococcus mutans in human dental decay. Microbiol Rev 1986;50:353–80.
[5] Jenkinson HF, Lamont RJ. Oral microbial communities in sickness and in health. Trends Microbiol 2005;13:589–95.
[6] Kolenbrander PE, Andersen RN, Blehert DS, Egland PG, Foster JS, Palmer Jr. RJ. Communication Among Oral Bacteria. Microbiol Mol Biol Rev 2002;66:486–505.
[7] Kuramitsu HK, He X, Lux R, Anderson MH, Shi W. Interspecies interactions within oral microbial communities. Microbiol Mol Biol Rev 2007;71:653–70.
[8] Kouidhi B, Al Qurashi YM, Chaieb K. Drug resistance of bacterial dental biofilm and the potential use of natural compounds as alternative for prevention and treatment. Micro Pathog 2015;80:39–49.
[9] Roberts AP, Mullany P. Oral biofilms: a reservoir of transferable, bacterial, antimicrobial resistance. Expert Rev Anti Infect Ther 2010;8:1441–50.
[10] Saini R, Saini S, Sharma S. Biofilm: a dental microbial infection. J Nat Sci Biol Med 2011;2:71–5.
[11] Bowden GH, Hamilton IR. Survival of oral bacteria. Crit Rev Oral Biol Med 1998;9:54–85.
[12] Quivey Jr RG, Kuhnert WL, Hahn K. Adaptation of Oral Streptococci to Low pH. Adv Micro Physiol 2000;42:239–74.
[13] Yamashita Y, Bowen WH, Burne RA, Kuramitsu HK. Role of the Streptococcus mutans gtf Genes in Caries Induction in the Specific Pathogen-free Rat Model. Infect Immun 1993;61:3811–7.
[14] Aoki H, Shiroza T, Hayakawa M, Sato S, Kuramitsu HK. Cloning of a streptococcus mutans glucosyltransferase gene coding for insoluble glucan synthesis. Infect Immun 1986;53:587–94.
[15] Hanada N, Kuramitsu HK. Isolation and characterization of the streptococcus mutans gtfC gene coding for synthesis of both soluble and insoluble glucans. Infect Immun 1988;56:1999–2005.
[16] Hanada N, Kuramitsu HK. Isolation and characterization of the streptococcus mutans gtfD gene coding for primer-dependent soluble glucan synthesis. Infect Immun 1989;57:2079–85.
[17] Monchois V, Willemot RM, Monsan P. Glucansucrases: mechanism of action and structure-function relationships. FEMS Microbiol Rev 1999;23:131–51.
[18] Ahirwar P, Kozlovskaya V, Nijampatnam B, Rojas EM, Pukkanasut P, Inman D, et al. Hydrogel-encapsulated biofilm inhibitors abrogate the cariogenic activity of streptococcus mutans. J Med Chem 2023;66:7909–25.
[19] Aframian DJ, Davidowitz T, Benoliel R. The distribution of oral mucosal pH values in healthy saliva secretors. Oral Dis 2006;12:420–3.
[20] Baliga S, Muglikar S, Kale R. Salivary pH: a diagnostic biomarker. J Indian Soc Periodo 2013;17:461–5.
[21] Bardow A., Pederson A.M.L., and Nauntofte B., Saliva. In: Miles TS, Nauntofte B, Svensson P eds. Clin Oral Physiol, 2004: p. 17–33.
[22] Lazarchik DA, Filler SJ. Effects of gastroesophageal reflux on the oral cavity. Am J Med 1997;103:107S–13S.
[23] Markitziu A, Aframian D. Gastro-intestinal disorders. Br Dent J 1997;182:207.
[24] Robb ND, Smith BG, Geidrys-Leeper E. The distribution of erosion in the dentitions of patients with eating disorders. Br Dent J 1995;178:171–5.
[25] Balhaddad AA, Kansara AA, Hidan D, Weir MD, Xu HHK, Melo MAS. Toward dental caries: exploring nanoparticle-based platforms and calcium phosphate compounds for dental restorative materials. Bioact Mater 2019;4:43–55.
[26] Carrouel F, Viennot S, Ottolenghi L, Gaillard C, Bourgeois D. Nanoparticles as anti-microbial, anti-inflammatory, and remineralizing agents in oral care cosmetics: a review of the current situation. Nanomaterials 2020;10:140.
[27] Chen H, Gu L, Liao B, Zhou X, Cheng L, Ren B. Advances of anti-caries nanomaterials. Molecules 2020;25:5047.
[28] Song W, Ge S. Application of antimicrobial nanoparticles in dentistry. Molecules 2019;24:1033.
[29] Zhao Z, Ding C, Wang Y, Tan H, Li J. pH-Responsive polymeric nanocarriers for efficient killing of cariogenic bacteria in biofilms. Biomater Sci 2019;7:1643–51.
[30] Sims KR, Maceren JP, Liu Y, Rocha GR, Koo H, Benoit DSW. Dual antibacterial drug-loaded nanoparticles synergistically improve treatment of streptococcus mutans biofilms. Acta Biomater 2020;115:418–31.
[31] Yi Y, Wang L, Chen L, Lin Y, Luo Z, Chen Z, et al. Farnesal-loaded pH-sensitive polymeric micelles provided effective prevention and treatment on dental caries. J Nanobiotech 2020;18:89.
[32] Seneviratne CJ, Leung KC-F, Wong C-H, Lee S-F, Li X, Leung PC, et al. Nanoparticle-encapsulated chlorhexidine against oral bacterial biofilms. Plos One 2014;9:e103234.
[33] Zhang JF, Wu R, Fan Y, Liao S, Wang Y, Wen ZT, et al. Antibacterial dental composites with chlorhexidine and mesoporous silica. J Dent Res 2014;93:1283–9.
[34] Nguyen S, Hiorth M, Rykke M, Smistad G. Polymer coated liposomes for dental drug delivery: interactions with parotid saliva and dental enamel. Eur J Pharm Sci 2013;50:78–85.
[35] Feitosa SA, Palasuk J, Kamocki K, Geraldeli S, Gregory RL, Platt JA, et al. Doxycycline-encapsulated nanotube-modified dentin adhesives. J Dent Res 2014;93:1270–6.
[36] Zhou Y, Yang J, Lin Z, Li J, Liang K, Yuan H, et al. Triclosan-Loaded Poly(amido amine) dendrimer for simultaneous treatment and remineralization of human dentine. Colloids Surf B 2014;115:237–43.
[37] Ferji K, Nouvel C, Babin J, Li MH, Gaillard C, Nicol E, et al. Polymersomes from amphiphilic glycopolymers containing polymeric liquid crystal grafts. ACS Macro Lett 2015;4:1119–22.
[38] Ghorbanizamani F, Moulahoum H, Zihnioglu F, Timur S. Nanohybrid carriers: the yin–yang equilibrium between natural and synthetic in biomedicine. Biomat Sci 2020;8:3237–47.
[39] Battaglia G, Ryan AJ. Bilayers and interdigitation in block copolymer vesicles. J Am Chem Soc 2005;127:8757–64.
[40] Agut W, Brulet A, Schatz C, Taton D, Lecommandoux S. pH and temperature responsive polymeric micelles and polymersomes by self-assembly of poly[2-(dimethylamino)ethyl methacrylate]-b-poly(glutamic acid) double hydrophilic block copolymers. Langmuir 2010;26:10546–54.
[41] Kita-Tokarczyk K, Grumelard J, Haefele T, Meier W. Block copolymer vesicles—using concepts from polymer chemistry to mimic biomembranes. Polymer 2005;46:3540–63.
[42] Liang X, Liu F, Kozlovskaya V, Palchak Z, Kharlampieva E. Thermoresponsive micelles from double LCST-Poly(3-methyl-N-vinylcaprolactam) block copolymers for cancer therapy. ACS Macro Lett 2015;4:308–11.
[43] Liu F, Kozlovskaya V, Zavgorodnya O, Martinez-Lopez C, Catledge S, Kharlampieva E. Encapsulation of anticancer drug by hydrogen-bonded multilayers of tannic acid. Softw Matter 2014;10:9237–47.
[44] Loo C, Corliss D, Ganeshkumar N. Streptococcus gordonii biofilm formation: identification of genes that code for biofilm phenotypes. J Bacteriol 2000;182:1374–82.
[45] Liu C, Worthington RJ, Melander C, Wu H. A new small molecule specifically inhibits the cariogenic bacterium streptococcus mutans in multispecies biofilms. Antimicrob Agents Chemother 2011;55:2679–87.
[46] Zhang Q, Nguyen T, McMichael M, Velu SE, Zou J, Zhou X, et al. New small-molecule inhibitors of dihydrofolate reductase inhibit streptococcus mutans. Int J Antimicrob Agents 2015;46:174–82.
[47] Huffines JT, Scoffield JA. Disruption of streptococcus mutans and candida albicans synergy by a commensal streptococcus. Sci Rep 2020;10:19661.
[48] Huffines JT, Stoner SN, Baty JJ, Scoffield JA. Nitrite triggers reprogramming of the oral polymicrobial metabolome by a commensal streptococcus. Front Cell Infect Microbiol 2022;12:833339.
[49] Schrödinger L., The PyMOL Molecular Graphics System, Version 2.4.2.
[50] BioSolveIT GmbH, SeeSAR version 13.0.1. 2023: Sankt Augustin, Germany.
[51] Rarey M, Kramer B, Lengauer T, Klebe G. A fast flexible docking method using an incremental construction algorithm. J Mol Biol 1996;261:470–89.
[52] Warren GL, Andrews CW, Capelli AM, Clarke B, LaLonde J, Lambert MH, et al. A critical assessment of docking programs and scoring functions. J Med Chem 2006;49:5912–31.
[53] Keyes PH. Dental caries in the molar teeth of rats. II. A method for diagnosing and scoring several types of lesions simultaneously. J Dent Res 1958;37:1088–99.

[54] Bruce-Keller AJ, Salbaum JM, Luo M, Blanchard Et, Taylor CM, Welsh DA, et al. Obese-type gut microbiota induce neurobehavioral changes in the absence of obesity. Biol Psychiatry 2015;77:607–15.
[55] Lu Y, Zhou G, Ewald J, Pang Z, Shiri T, Xia J. MicrobiomeAnalyst 2.0: comprehensive statistical, functional and integrative analysis of microbiome data. Nucleic Acids Res 2023;51:W310–8.
[56] Zhang Q, Ma Q, Wang Y, Wu H, Zou J. Molecular mechanisms of inhibiting glucosyltransferases for biofilm formation in streptococcus mutans. Int J Oral Sci 2021;13:30.
[57] Banas JA, Lynch DJ, Michalek SM, Zhu M, Drake D, Qian F. Cariogenicity of Streptococcus mutans Glucan-Binding Protein Deletion Mutants. Oral Health Dent Manag 2013;12:191–9.
[58] Hazlett KR, Michalek SM, Banas JA. Inactivation of the gbpA Gene of streptococcus mutans increases virulence and promotes in vivo accumulation of recombinations between the glucosyltransferase B and C Genes. Infect Immun 1998;66:2180–5.
[59] Michalek SM, McGhee JR, Navia JM. Virulence of Streptococcus mutans: a sensitive method for evaluating cariogenicity in young gnotobiotic rats. Infect Immun 1975;12:69–75.
[60] Michalek SM, McGhee JR, Shiota T, Devenyns D. Virulence of Streptococcus mutans: cariogenicity of S. mutans in Adult Gnotobiotic Rats. Infect Immun 1977; 15:466–71.
[61] Palmer SR, Crowley PJ, Oli MW, Ruelf MA, Michalek SM, Brady LJ. YidC1 and YidC2 are functionally distinct proteins involved in protein secretion, biofilm formation and cariogenicity of Streptococcus mutans. Microbiology 2012;158: 1702–12.
[62] Yang Y, Kozlovskaya V, Dolmat M, Song Y, Qian S, Urban VS, et al. Temperature controlled transformations of giant unilamellar vesicles of amphiphilic triblock copolymers synthesized via microfluidic mixing. Appl Surf Sci Adv 2021;5:100101.
[63] Yang Y, Kozlovskaya V, Zhang Z, Xing C, Zaharias S, Dolmat M, et al. Poly(N-vinylpyrrolidone)-block-Poly(dimethylsiloxane)-block-Poly(N-vinylpyrrolidone) Triblock Copolymer Polymersomes for Delivery of PARP1 siRNA to Breast Cancers. ACS Appl Bio Mater 2022;5:1670–82.
[64] Liu F, Kozlovskaya V, Medipelli S, Xue B, Ahmad F, Saeed M, et al. Temperature-sensitive polymersomes for controlled delivery of anticancer drugs. Chem Mater 2015;27:7945–56.
[65] Kozlovskaya V, Yang Y, Liu F, Ingle K, Ahmad A, Halade GV, et al. Dually Responsive Poly(N-vinylcaprolactam)-b-poly(dimethylsiloxane)-b-poly(N-vinylcaprolactam) Polymersomes for Controlled Delivery. Molecules 2022;27: 3485.
[66] Guo L, McLean JS, Yang Y, Eckert R, Kaplan CW, Kyme P, et al. Precision-guided antimicrobial peptide as a targeted modulator of human microbial ecology. Proc Natl Acad Sci USA 2015;112:7569–74.
[67] Garcia SS, Blackledge MS, Michalek S, Su L, Ptacek T, Eipers P, et al. Targeting of streptococcus mutans biofilms by a novel small molecule prevents dental caries and preserves the oral microbiome. J Dent Res 2017;96:807–14.